Petrogenesis of lavas from Volcano Azufre, Northern Chile: evidence for crustal input

James Lister

Contents

List of Figures

1 Abstract

Magmatism that occurs within the Central Volcanic Zone (CVZ) of the Andes is heavily influenced by processes of differentiation and assimilation that occur within the extremely thick continental crust. These processes, that result in crustal contamination of mantle derived magmas, are not uniform across the region and are determined locally. Data from Azufre is combined with that of previously studied volcanoes of the CVZ, and specifically the Altiplano-Puna Volcanic Complex (APVC) in northern Chile, to further understand such processes that have occurred in this region. Factors that need to be taken into consideration when examining volcanoes of the APVC are the aforementioned thickness of the continental crust of the Andes, which differentiates the Andes from other volcanic arcs globally, and the presence of a zone of low seismic velocity (with up to 20% partial melt), the Altiplano-Puna Magma Body (APMB), below the APVC as they could both have had a major effect on erupting lavas. Elemental concentration and isotope data are used here to examine the role that the APMB has had on the evolution of Azufre. This data set is also compared to those of previously studied volcanoes of the APVC to further provide understanding as to the interaction between the APMB and the APVC. Major element data reveals well defined sub-alkaline trends, with samples predominantly being andesitic in composition. $^{87}Sr/^{86}Sr$ ratios of 0.7067 - 0.7075 and δ ^{18}O values of 7.85 - 9.72 are high in comparison to those of other Central Andean lavas, however in comparison to other erupted lavas of the APVC they are low. A transition from the edges of the APVC towards the centre show an increase in $^{87}Sr/^{86}Sr$ and δ ^{18}O. Conversely $^{143}Nd/^{144}Nd$ ratios decrease towards the centre, with Azufre displaying ratios of 0.5123 - 0.5124. These changing ratios from the edge to centre of the APVC correspond with changing thickness of the APMB below the APVC and are therefore viewed to represent the amount of interaction between parental magmas of the APVC with the partial melt of the APMB, primarily with increasing $^{87}Sr/^{86}Sr$ indicating increasing amounts of interaction. δ ^{18}O data indicates that there are multiple sources of O enrichment, evidenced by two opposite data arrays, with one array indicating assimilation by magmas of high δ ^{18}O crust and the second array indicating assimilation of low δ ^{18}O crust. Modelling of δ ^{18}O suggests that the magmas which have assimilated low δ ^{18}O crustal material have interacted with between -2.01 and 3.49 ‰. Low LREE/HREE ratios and a negative Eu anomaly support the idea that assimilation of crustal material occurred at shallow crustal levels by indicating shallow plagioclase fractionation and evolution in a garnet free environment, most likely within the APMB.

2 Introduction

Azufre volcano is situated within the Central Volcanic Zone (CVZ) of the Andes, a zone which extends from latitude 14°S to 28°S, and is part of a chain of relatively unstudied volcanoes which runs parallel, and to the north of, the San Pedro – Linzor volcanic chain (SPLVC). The CVZ is one of three major active volcanic zones along this margin (the other two being the Northern and Southern Volcanic Zones) and was formed as the result of the latest cycle of volcanism in the Central Andes (Davidson et al., 1990; de Silva, 1989; Godoy et al., 2017). Subduction of the Nazca plate below the South America plate steepened from 10° to 30° during the Miocene – Holocene, resulting in the active volcanic arc being mainly located in the Western Cordillera. The northern boundary of the CVZ coincides with the edge of the subducted Nazca Ridge, while the southern boundary coincides with the Juan Fernandez ridge. Both of these ridges subduct below the South American plate at shallow angles (Godoy et al., 2014; Mamani et al., 2010). Lucassen et al. (2001) refer to the Central Andes as "the type example of a magmatic arc on continental crust and of a subduction-driven orogeny with overthickened crust", where the second part of the statement refers to the 70km thick section of continental crust which the Central Andes are situated on. This section of continental crust is viewed as overthickened, as arcs generally have crustal thicknesses that are <40km (Davidson et al., 1990; de Silva, 1989; Godoy et al., 2014, 2017; Mamani et al., 2010). This exceptionally thick continental crust of the Central Andes corresponds with the rocks of the CVZ being strongly enriched in incompatible trace elements and isotopically distinct from the rest of the Andes. There are multiple different theories as to the cause for these characteristics, however the theory investigated by this research is that there is either fractional crystallisation, crustal assimilation during magma ascent, or a combination of the two processes (Davidson et al., 1990; Godoy et al., 2014; Mamani et al., 2010).

The presence of geophysical anomalies indicates that there is a region in the upper crust (∼4 – 30 km) which is partially-molten. This region, known as the Altiplano-Puna Magma Body (APMB) is largely consistent with the Altiplano-Puna Volcanic Complex (APVC), the large ignimbrite province which makes up a large portion of the CVZ, and is theorised to either be the parent magma body for APVC or the parent body for an intermediate magma accumulation zone which could have supplied an upper-crustal sub-volcanic system (Chmielowski et al., 1999; de Silva, 1989; de Silva & Gosnold, 2007; Godoy et al., 2014, 2017; Ward et al., 2014). This study presents isotopic and elemental data to characterise Azufre and compare it to the published data of the San Pedro – Linzor volcanic chain. From this comparison we aim to draw conclusions regarding whether any assimilation of crustal material has occurred during the ascent of magma through the thick continental crust. High $^{87}Sr/^{86}Sr$ isotopic ratios, >0.706, are observed in lavas of the Central Andes, indicating that crustal contamination is present in other volcanoes previously studied in this region (Davidson et al., 1990; Godoy et al., 2014; Lucassen et al., 2001).

The processes which led to the thickening of the Andean crust are still not well understood. The difficulty comes due to the scarcity of primary basalts in regions of thick continental crust, making it more difficult to determine to what degree the crust has interacted with primary magmas as they ascended. The combination of Sr and O isotope, as well as major and trace element,

data analysis provides an approach that can be used to help further our understanding of these processes, as they are used to show that the erupted lavas are hybrid melts of enriched mantle and crust. A thick crust should result in a garnet signature, due to its role in high-pressure magmatic differentiation and/or assimilation, however this feature is absent in the lavas of the CVZ, in addition K_2O contents, and other incompatible trace elements, are expected to increase with increasing continental crustal thickness (Dickinson, 1975; Godoy et al., 2014; Michelfelder et al., 2013). The lack of a garnet signature in the rocks of the APVC indicate that magma evolution occurred at shallow depths in the crust as opposed to the deep in the crust. When these data are looked at in the context of the APVC the role of the APMB becomes striking in its importance. The presence and nature of the APMB can potentially provide an explanation for the signatures of the erupted lavas observed in the APVC (Godoy et al., 2017).

The aims of this study are:

- to use geochemical (major and trace element) and isotopic (radiogenic and stable) data to look at:
  - (i) potential sources of magma
  - (ii) magmatic evolution
- to identify any similarities between the trends observed at Azufre and the those of the San Pedro — Linzor Volcanic Chain, Aucanquilcha, Ollague, and Uturuncu.

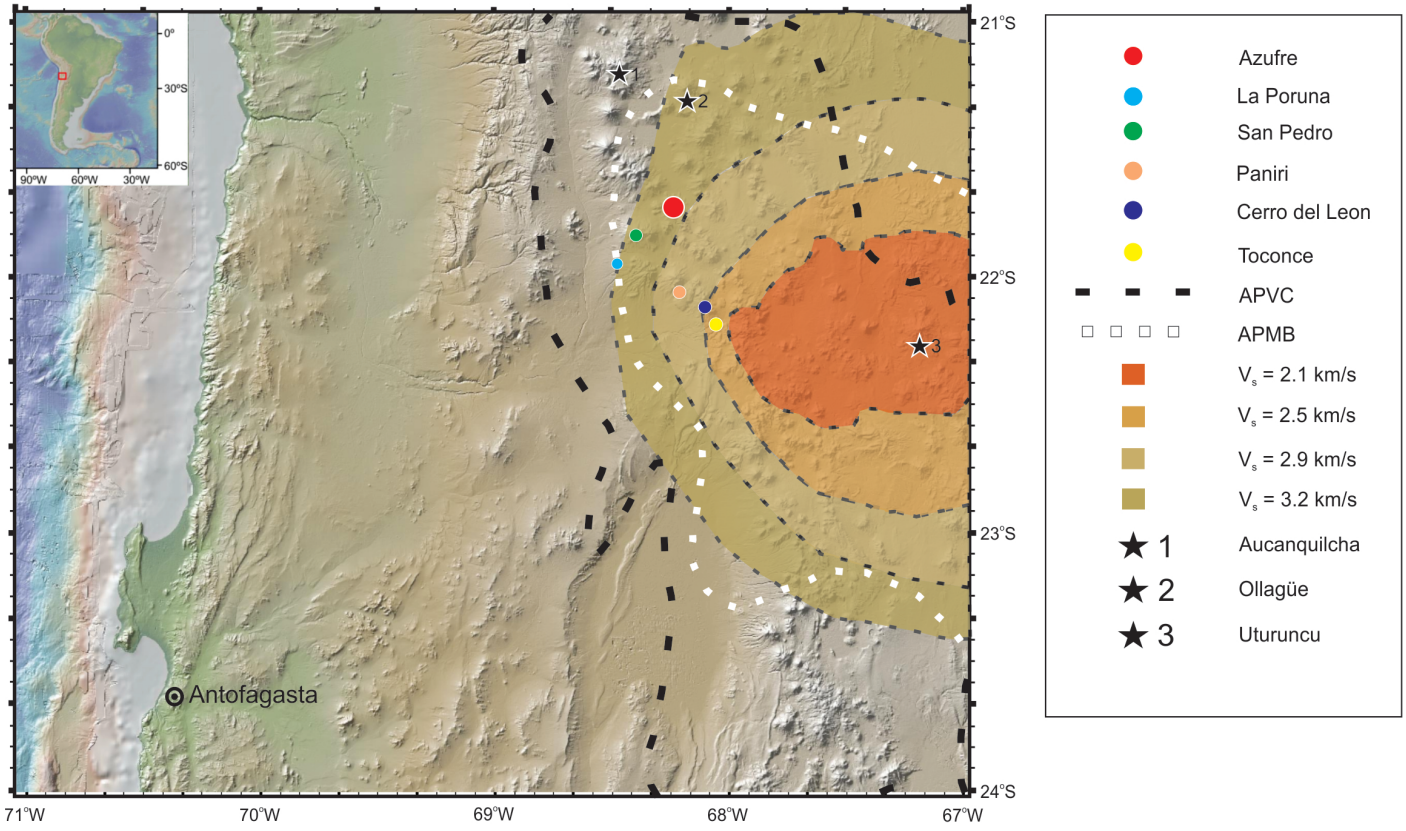

Figure 1: GlobalMulti-Resolution Topography image after Godoy et al. (2017)

3 Geological Setting

Azufre is located at, approximately, 68°14'W and 21°47'S. This situates it within the Central Volcanic Zone (CVZ) of the Central Andes, which extends from latitude 14°S to 28°S, and at the very north of the Altiplano-Puna Volcanic Complex (APVC), which extends from 21°S to 24°S (Fig. 1) (Allmendinger et al., 1997; Schurr et al., 2003; Zandt et al., 2003).

3.1 Altiplano-Puna Plateau

The Altiplano-Puna plateau is situated between the active chain of volcanoes, that are the western Cordillera, and the eastern Cordillera, which was formed by crustal shortening. It is a broad, elevated plateau (>3600-4000m a.s.l.) with crustal thicknesses up to 70km. The Altiplano and Puna are internally draining basins which, together, form this plateau. The plateau was formed during a period of intense shortening, in the late Oligocene and Miocene, due to the subduction of the Nazca plate below the South American plate. This subduction is occurring at an angle of ∼30° and at a rate of 65mm/yr (Allmendinger et al., 1997; Beck et al., 1996; Freymuth et al., 2015; Godoy et al., 2014; Mamani et al., 2008; McQuarrie et al., 2005; Michelfelder et al., 2013; Schurr et al., 2003).

3.2 Altiplano-Puna Volcanic Complex

The APVC is located at the transition between the Altiplano and Puna plateaus and is, most recently, characterised by extensive ignimbrite eruptions, which have led to the formation of large, silicic calderas. Ignimbrite flare-ups are found regionally, however the APVC represents the most intense node of these events. The APVC covers approximately 50 000 km^2 within the CVZ (Chmielowski et al., 1999; De Silva & Kay, 2018; Leidig & Zandt, 2003; Michelfelder et al., 2013; Prezzi et al., 2009; Zandt et al., 2003). A suggested reason for the ignimbrite flare ups which characterise the APVC is partial crustal melting. Geophysical anomalies beneath the Altiplano-Puna plateau, such as high surface heat flow and the presence of a broad highly conductive zone in the middle crust, are indicators to this being the case (Chmielowski et al., 1999; de Silva, 1989; de Silva & Gosnold, 2007; Schurr et al., 2003). Volcanism since the Pliocene has been predominantly mafic, with the formation of stratovolcanoes building onto the basement formed by the previous ignimbrite flare up (de Silva et al., 1994; Kay et al., 1994, 1996; Schurr et al., 2003).

Azufre falls into the Antofalla crustal domain, one of 4 areas characterised by Pb isotope values, the crust of which is dominantly felsic. The Antofalla Domain has $^{206}Pb/^{204}Pb$ values >18.551. These domains are Proterozoic or Paleozoic in age, however they relate to Mesozoic and younger rocks due to either emplacement into the older basement or traversal (and therefore assimilation) through it (Aitcheson, 1995; Godoy et al., 2014; Mamani et al., 2008, 2010). Parental magmas for lavas in the APVC are generally either incompatible trace element enriched basalt (EB) or medium-K calcalkaline basaltic andesite (BA), with the northern Altiplano region a combination of the two and the southern Puna region dominated by BA type magma (Blum-Oeste & Wörner, 2016). Davidson et al. (1990) use the terms "parental" magma or "baseline" to describe the most mafic composition erupted for the region.

3.3 Altiplano-Puna Magma Body

The APMB is a region of the crust situated below the APVC, and is theorised to be the source of the large ignimbrite flare ups in the area. It is a regionally extensive sill-like magma body situated in the mid-crust (Zandt et al., 2003). It is through the combined analysis of various geophysical data that the APMB has been defined. Zones of high electrical conductivity situated between 10 and 30km below the APVC, a low velocity zone, at a depth between 10 and 20km, is indicated by seismic refraction investigations, and the presence of highly developed anisotropy in the upper 20km of the crust. The bounds of these zones are depicted in Fig. 1 (Chmielowski et al., 1999; Zandt et al., 2003).

Zandt et al. (2003) constrained the APMB's size to be approximately 3° in longitude 2° in latitude, and area of around 60 000km^2. This area roughly overlaps with the APVC, illustrated in Fig. 1,and this correlation, coupled with the silicic nature of the ignimbrite sheets in the APVC strengthen the case that the APMB is associated with silicic magma (Chmielowski et al., 1999; Godoy et al., 2014). Allmendinger et al. (1997) further assert that the low average velocity of the crust below the Altiplano and the Poisson's Ratio of 0.25 imply that the crust is felsic in composition.

The APMB is most likely a magma storage chamber, as magma prdouction is due to melting of the lower crust (de Silva, 1989; de Silva et al., 2006; Chmielowski et al., 1999; Kay et al., 2010; Schmitt et al., 2001).

3.4 Crustal Thickening, Crustal Melting, And Origin Of The Ignimbrite Magmas

The thickness of the continental crust below the Central Andes is fairly well established due to refraction experiments, broadband passive recording of earthquakes in the subducted plate, and modeling of the gravity field (Allmendinger et al., 1997). Crustal melting is intrinsically linked to crustal thickening. Between 10-12Ma the Andean crust underwent thickening, as a response to the E-W tectonic shortening that occurred as the subduction angle of the Nazca Plate steepened from 10° to 30°. Related to this subduction was the invasion of the crust by basaltic magmas, evidenced by a dipping low velocity zone which overlies the Nazca plate and which decreases in intensity with depth (Baumont et al., 2002; de Silva, 1989; Godoy et al., 2014; Zandt et al., 2003). The process of crustal thickening occurred in 2 stages. Stage 1 involved uplift of the Altiplano and Puna segments of the Altiplano-Puna plateau at 25Ma and between 15-20Ma respectively, due to thinning and thermal softening of the lithosphere caused by the aforementioned subduction. Stage 2 involved shortening ceasing in the Altiplano and moving eastward between 12-6Ma while continuing in the Puna until 2-1Ma (Allmendinger et al., 1997). During the process of crustal thickening the lower crust becomes subjected to increasing lithostatic pressure, which in turn leads to the formation of garnet at the expense of plagioclase. The presence of garnet versus plagioclase is identified by the Sr/Y, La/Yb, and La/Sm ratios as Y, Yb, and Sm have an affinity for garnet. The presence of garnet and the absence of plagioclase is therefore identified by high Sr/Y, La/Yb, and La/Sm ratios respectively. Low ratios conversely reflect the absence of garnet

and the presence of plagioclase. This feature is observed in the volcanoes of the SPLVC (Godoy et al., 2014; Mamani et al., 2010).

3.5 Lineaments and Tectonic Setting

Tibaldi et al. (2009) outline a lineament that strikes NW through Azufre and has the same strike as the system of normal faults that run through the volcanoes to the SE of Azufre. These systems of faults are suggested to be linked to the transport of magma, as the distribution of stratovolcanoes indicates that magma used well established conduits. The connection between the stratovolcanoes and the fault systems of the APVC is made due to the processes of faulting and plutonism being interrelated. Magmatic heat weakens the crust, localising strain, while well established conduits act to focus the ascent of the magma (Chernicoff et al., 2002; Tibaldi et al., 2009). de Silva et al. (1994) suggest that the NW-SE faulting that apparently controls volcanic centre location is related to the southern margin of the Pastos Grandes caldera complex (located to the East of Azufre). The last 1-2Ma have been dominated by strike-slip and extensional faulting, whereas the history of the region is generally of thrust faulting (Allmendinger et al., 1997; Baby et al., 1990). The volcanic chain, of which Azufre is a part, has an orientation that is parallel to three major regional lineaments. These lineaments are the Lípez-Coranzuli, Pastos-Grandes and Calama-Olacapato-El Toro fault systems, and are interpreted to have been reactivated by the extensional regime that is related to principal stress direction changes during the Miocene-Pliocene, from vertical crustal thickening to orogen parallel stretching, caused by the emplacement of tabular intrusions (Godoy et al., 2014; Riller et al., 2001; Tibaldi et al., 2009; Trumbull et al., 2006; Zandt et al., 2003).

4 Methods

4.1 Sample Collection

Initial sample collection, in April 2016, resulted in 12 samples being collected from separate lava flows situated on the northern slopes of Azufre. Lava samples were split and then crushed, using a jaw crusher, at the Universidad Catolica del Norte Chile before being separated into two batches, the first of which to remain in Chile to be analysed by Quantitative Evaluation of Minerals by Scanning electron microscopy (QEMSCAN). The second sample batch was transported to the University of Cape Town (UCT) for further processing and analysis by: X-Ray Fluorescence, Multi Collector Inductively Coupled Plasma Mass Spectrometry (MC-ICP-MS), Inductively Coupled Plasma Mass Spectrometry (ICP-MS), and Laser Fluorination.

A second suite of 7 samples was collected in April 2017, by Doctors Petrus Le Roux and Benigno Godoy, and Professor Chris Harris. The process of preparation was the same for both sets of samples, except for the first set being crushed at the Universidad Catolica del Norte Chile and the second set being crushed at UCT.

4.2 Sample Preparation

At UCT the crushed samples were separated to prepare a set for mineral picking, for $\delta\ ^{18}O$ analyses, and a set for XRF and ICP-MS analysis. The samples were sieved using a stack of sieves with 1000μm and 650μm meshes to produce mesh fractions, with the set for XRF and ICP-MS analysis then being milled to produce powder.

Table 1: Azufre Sample Locations, Longitude and Latitude

Sample	Longitude	Latitude
JL-AZU-001	-68.269806	-21.722556
JL-AZU-002	-68.267194	-21.719361
JL-AZU-003	-68.185639	-21.746472
JL-AZU-004	-68.179917	-21.747583
JL-AZU-005	-68.199806	-21.725917
JL-AZU-006	-68.242222	-21.737583
JL-AZU-007	-68.277417	-21.727833
JL-AZU-008	-68.277167	-21.745361
JL-AZU-009	-68.285194	-21.744194
JL-AZU-010	-68.279417	-21.756639
JL-AZU-011	-68.278889	-21.754278
JL-AZU-012	-68.284361	-21.763056
AZU-17-001	-68.298262	-21.820779
AZU-17-002	-68.239511	-21.832281
AZU-17-004	-68.238683	-21.833316
AZU-17-005	-68.212994	-21.820647
AZU-17-006	-68.206914	-21.81078056
AZU-17-008	-68.226340	-21.798387
AZU-17-011	-68.301572	-21.816583

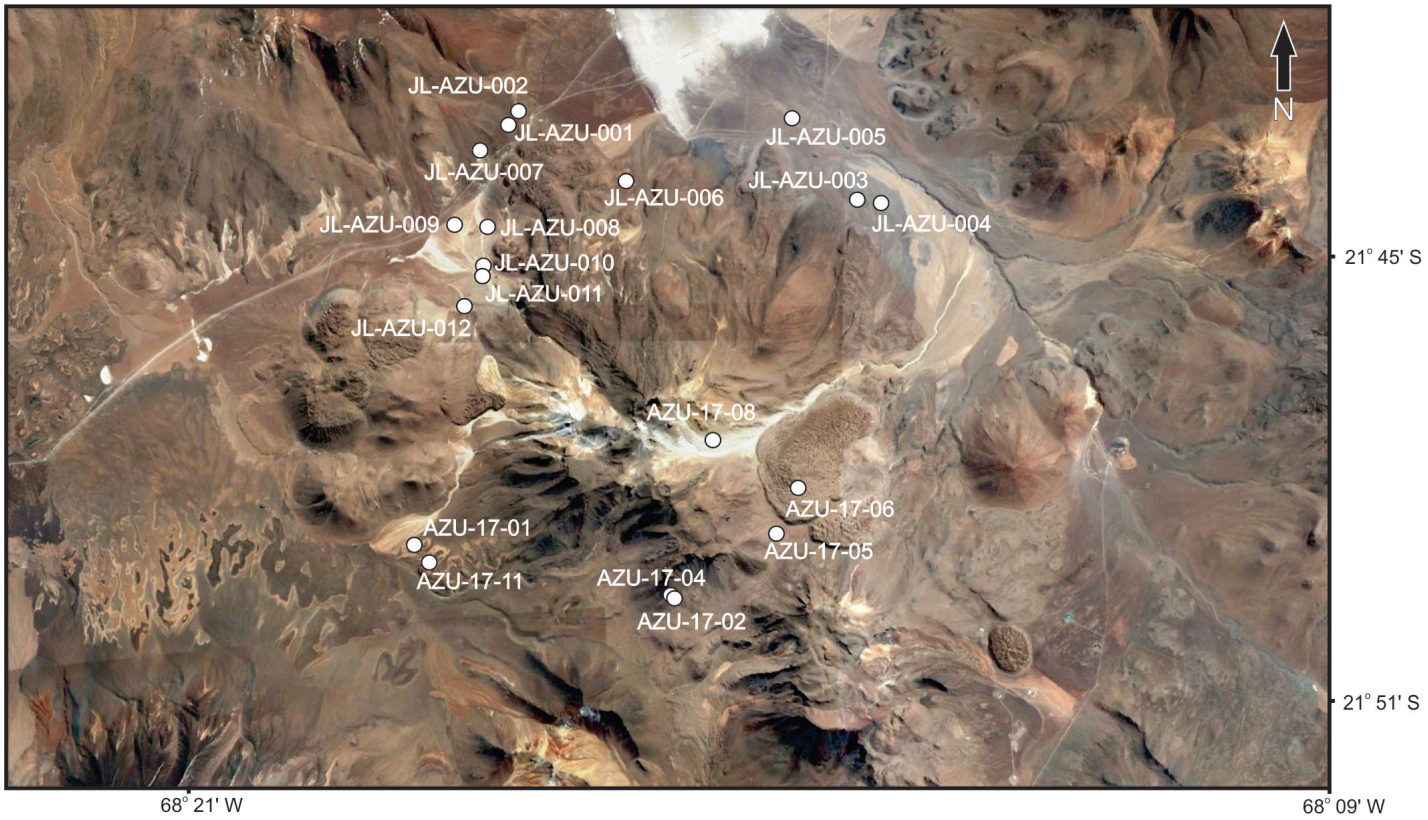

Figure 2: Satellite image of the study area showing the location of samples.
21°52'41.55"S and 68°20'17.23"W. **Google Earth**. May 05, 2016. November 07, 2016.

4.3 Preparation for XRF analysis

4.3.1 Claisse-Fluxy Fusion Discs

For XRF analysis fusion discs, of each sample, are prepared. Approximately 2g of powdered sample is added to a crucible of known mass, before re-weighing. The samples are then dried in an oven, at 110°C, for at least 4 hours. Once cooled, the samples are re-weighed and then put into a furnace at a temperature between 850-1000°C overnight. Samples are re-weighed a final time before being transferred from crucibles to small glass vials that are sealed with mylar film and a lid.

Lithium tetraborate/metaborate flux is dried in a furnace at 450°C overnight. Once cooled, 6g of flux, to act as a releasing agent, and 0.7g of sample are measured into labelled vials and sealed with mylar film and a lid. The flux and sample are fused in a Claisse gas burner in order to form fusion discs.

4.3.2 XRF pellets

6g of powdered sample is weighed out and mixed 3 drops of binding agent. The sample and the binding agent are mixed thoroughly before being poured into a mould (a combination of a hollow tube within a larger mould) where a small amount of pressure is applied to form the initial shape of the pallet and the tube is then removed. A small test tube of boric acid is added to the mould and a cylinder is inserted into the mould on top of the combination of sample and acid. The mould is then placed in a hydraulic press and 10 tons of pressure are applied to it. The pellet is carefully removed from the mould and labelled.

4.4 XRF Analysis

All samples were analysed for whole rock major oxides and trace elements using X-ray Flurescence Spectrometry (XRF). The analyse were performed using a Panalytical Axios XRF spectrometre, in the Department of Geological Sciences at the University of Cape Town. Analyses of major oxides and trace elements are performed separately, but both are calibrated using a series of well characterised standards, from natural rock powders, that are issued by organisations such as MINTEK, the United States Geological Survey, and the Geological Society of Japan. These standards were prepared identically as the samples that were being analysed. Elemental concentrations in unknowns are obtained through the use of calibration curves versus measured analyte peak intensities, which are corrected for background. Absorption and enhancement effects were corrected through the use of iterative correction routines, which employ mass attenuation coefficients. Spectral line overlaps were corrected through the use of routines that are based on spiked blank analyses.

4.5 Sr and Nd analysis

4.5.1 Separation chemistry

Approximately 50mg of sample was weighed into 7ml Teflon beakers, after which 4ml of 4:1 2B conc. HF:HNO_3 was added to each sample and the beakers were then closed to digest on a hotplate, at 140°C. After 48 hours, the beakers were carefully opened to dry down at 140°C. Approximately 2ml of 65% 2B HNO_3 was added to the residue which remained in the beaker. This step is repeated so as to drive off fluorides. This solution was left to dry and then the samples were cooled and re-dissolved in 1.7ml of 2M 2B HNO_3. Samples are then split quantitatively by weight into 0.2ml and 1.5ml quantities for ICPMS and Sr and Nd elemental separation chemistry, respectively.

Sequential Sr and Nd separation chemistry of Míková & Denková (2007) was followed after Pin & Santos Zalduegui (1997). Two racks of vials were set up, one for Sr.Spec and one for Tru.Spec (TRansUranic-element Specific). Waste beakers are situated underneath each column in both racks. The initial step wass to open and condition the columns by adding 2 x 1ml 2M HNO_3 to each column. The racks are then assembled so that the Sr.Spec rack was situated above the Tru.Spec rack. This new set up wass then conditioned with 1ml 2M HNO_3 before loading 1.45ml

of the sample. Following loading of samples the columns were rinsed with 1 x 0.5ml 2M HNO_3 and then washed with 4 x 0.5ml 2M HNO_3. The racks were then separated again and waste beakers situated under all the columns once again. After separation, the columns were washed, again, with 2 x 0.5ml 2M HNO_3. The waste beakers below the Sr.Spec columns were then swapped out for clean, labelled 7ml teflon beakers and Sr was collected with 6 x 0.5ml MQ water. Following separation, the Sr fraction was dried down, cooled, and had 2ml 0.2% HNO_3 added to it, before being ultrasonicated for 30 mins.The Sr.Spec columns were then ready for cleaning.

The Tru.Spec columns were rinsed with 0.25ml 0.05M HNO_3. A new rack was set up for Ln.Spec and this was opened and conditioned with 2 x 1ml 0.05M HNO_3. The racks were then assembled so that the Tru.Spec rack was situated above the Ln.Spec rack. This new set up was washed with 6 x 0.5ml 0.05M HNO_3 before being separated once again with the Tru.Spec columns ready for cleaning and the Ln.Spec columns were ready for collection. The Ln.Spec columns were rinsed with 2 x 0.5ml 0.05M HNO_3 and then again with 8ml 0.25M HCl. The waste beakers below the Ln.Spec columns were then swapped out for clean, labelled 15ml teflon beakers and Nd was collected with 7ml 0.25M HCl. The Ln.Spec columns were then ready for cleaning. Following separation, the Nd fraction was dried down and converted to nitrate with 1ml 2B HNO_3. This was repeated and the fraction was then cooled before 2ml 2% HNO_3 was added, before being ultrasonicated for 30 mins.

4.5.2 MC-ICP-MS Analysis

All isotope analyses were performed on a Nu Instruments NuPlasma HR in the MC-ICP-MS facility, housed in the Department of Geological Sciences, University of Cape Town, Rondebosch, Cape Town. Sr is analysed as 200ppb 0.2% HNO_3 solution using NIST SRM987 as the reference standard, with a normalising value for $^{86}Sr/^{88}Sr$ of 0.710255. Sr data is corrected for Rb interference, using the measured signal for ^{85}Rb and the natural $^{85}Rb/^{87}Rb$ ratio, and instrumental mass fractionation, using the exponential law and a $^{86}Sr/^{88}Sr$ value of 0.1194. Nd is analysed as 50ppb 2% HNO_3 solutions using Nu Instruments DSN-100 desolvating nebuliser using JNdi-1 as reference standard. The normalising value of JNdi-1, for $^{143}Nd/^{144}Nd$, is 0.512115. Nd isotope data are corrected for Sm and Ce interference, using the measured signal for ^{147}Sm and ^{140}Ce and the natural Sm and Ce isotope abundances, and instrumental mass fractionation, using the exponential law and a $^{146}Nd/^{144}Nd$ value of 0.7219.

4.6 Oxygen Isotopes

Oxygen isotope analysis were performed on quartz by laser fluorination following the methods described by Harris & Vogeli (2011). The system uses a 20 W New Wave CO_2 laser, which is mounted on a moveable stage, and takes a normal load of 10 samples (approximately 1 to 3 mg of quartz per sample) and 2 standards in a highly polished sample holder made of pure Ni.

Samples are loaded into the sample holder and then placed into an at 110°C for at least an

hour, after which they are moved into a reaction chamber. In the reaction chamber the samples are exposed to 10Kpa of BrF_5 in two rounds, after the chamber has been pumped for >2 hours. The first exposure is for a period of 30 seconds following which the BrF_5 is removed cryogenically and the chamber is pumped again (>30 minutes) before the second exposure, where the BrF_5 is left in the chamber overnight. Once the reaction has been completed any excess BrF_5, and free Br that has formed by disassociation, are frozen into a cold finger and the remaining gases are allowed to pass through a KCl trap that is maintained at about 200°C. This is order to remove any F_2 that has been produced.

Purified O_2 is collected onto 5 $\mathring{A}$ molecular sieves, which are contained in glass bottles for storage, by expanding the gasses, from the previous stage, into a stainless steel double-U trap which is immersed in liquid nitrogen.

4.7 Electron Microprobe

Electron microprobe analyses were conducted with a JEOL Superprobe JXA-8100 Electron Microprobe using wavelength dispersive spectrometers (WDS), on previously prepared polished sections. The electron beam was set to an accelerating potential of 15 kV, a beam current of 20 nA, and a 1-3 m diameter.

5 Petrography

The lava samples are medium grained and have porphyritic textures with approximately 40% to 55% by volume phenocrysts. Plagioclase is the most abundant phenocryst phase observed in the samples, amounting to between 50% to 70% of the mineral assemblage. Plagioclase phenocrysts display both simple and lamellar twinning, as well as oscillatory zoning. Other phenocryst phases present include orthopyroxene, clinopyroxene, biotite, hornblende, olivine, and an opaque mineral. These are not universal, however, and the quantities of minerals tend to vary between samples with several samples containing phases that are not present in other samples (this is primarily true of olivine).

Samples JL-AZU-001, JL-AZU-003, and JL-AZU-011 contain glomerocrysts. JL-AZU-001 contains glomerocrysts of plagioclase, biotite, and orthopyroxene, JL-AZU-003 contains plagioclase, orthopyroxene, and clinopyroxene, and JL-AZU-011 contains orthopyroxene and clinopyroxene.

Oscillatory zoning in plagioclase phenocrysts indicates that there was repeated injection of fresh, basic, magma into the chamber of already differentiated and cooled magma, which caused resorption of already crystallised plagioclase. The medium grain size and high propensity of felsic minerals indicates shallow crystallisation and interaction between mantle magmas and the crust respectively.

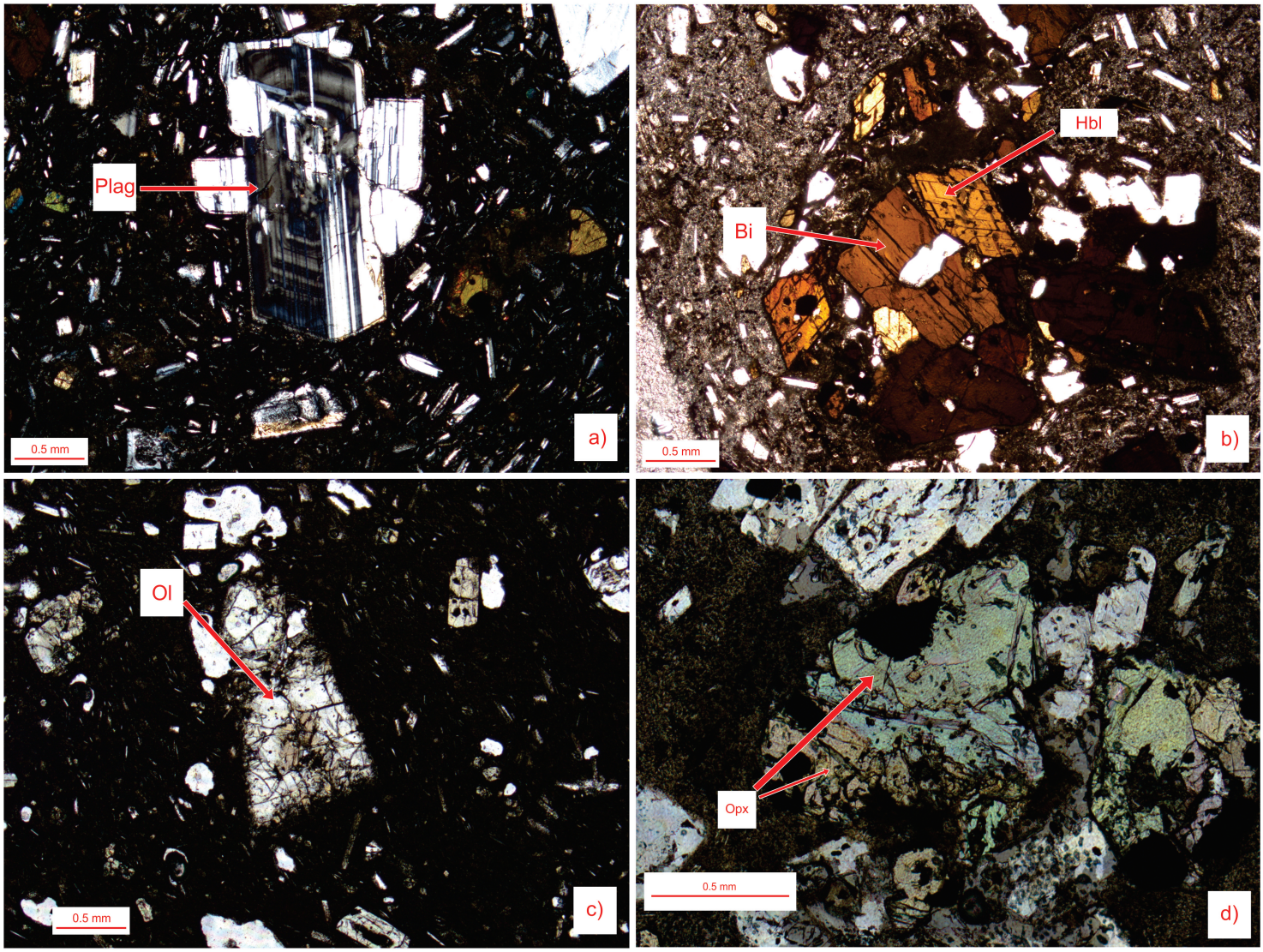

Figure 3: Pictomicrographs of samples from Azufre. (a) Plagioclase phenocryst exhibiting oscillatory zoning and lamellar twinning, in XPL (JL-AZU-002); (b) Glomerocryst composed of biotite and hornblende phenocrysts (JL-AZU-002); (c) Olivine phenocryst (JL-AZU-009); And (d) a glomerocryst composed of orthopyroxene phenocrsyts (JL-AZU-004). Evident in all samples is a glassy groundmass.

Table 2: Petrographic Descriptions for samples from Azufre

Sample	Mineral	Modal %	Grain size (mm)	Description	Texture	Rock type
JL-AZU-001					Hypocrystalline & porphrytic, with glomerocrysts of plagioclase, biotite, and orthopyroxene	Andesite
	Plagioclase (Plag)	25	<4	Subhedral to euhedral, lamellar & simple twinning, oscillatory zoning		
	Orthopyroxene (Opx)	5	<3	Anhedral to subhedral		
	Biotite (Bi)	5	<2	Anhedral to subhedral		
	Hornblende	5	<1	Subhedral to euhedral		
	Groundmass	60		Plag, bi, clinopyroxene (cpx), opx, and glass		
JL-AZU-002					Hypocrystalline & porphyritic, with fractured cpx xenoliths	Andesite
	Plagioclase	25	<3	Anhedral to euhedral, lamellar & simple twinning, oscillatory zoning		
	Biotite	10	<3	Anhedral to subhedral		
	Hornblende	10	<1	Subhedral to euhedral		
	Clinopyroxene	5	<3	Anhedral to euhedral		
	Opaque	<5	<1	Anhedral		
	Groundmass	50		Plag, magnetite, cpx, glass		
JL-AZU-003					Hypocrystalline & porphyritic, with glomerocrysts of plag, opx and cpx	Andesite
	Plagioclase	30	<4	Anhedral to euhedral, lamellar & simple twinning, oscillatory zoning		
	Biotite	15	<3	Anhedral to subhedral		
	Clinopyroxene	5	<1	Anhedral		
	Orthopyroxene	5	<1	Anhedral		
	Opaque		<1	Anhedral		
	Groundmass	45		Plag, opaques, glass		

Sample	Mineral	Modal %	Grain size (mm)	Description	Texture	Rock type
JL-AZU-004					Hypocrystalline & porphyritic	Dacite
	Plagioclase	35	<3	Anhedral to euhedral, lamellar & simple twinning, oscillatory zoning		
	Orthopyroxene	<5	<2	Anhedral to subhedral		
	Clinopyroxene	<5	<2	Anhedral to subhedral		
	Biotite	<5	<2	Anhedral to subhedral		
	Hornblende	<5	<1	Anhedral to subhedral		
	Opaque	5	<1	Anhedral		
	Groundmass	50		Plag, glass		
JL-AZU-005					Hypocrystalline & porphyritic	Andesite
	Plagioclase	35	<5	Anhedral to euhedral, lamellar & simple twinning, oscillatory zoning		
	Biotite	5	<5	Anhedral to subhedral		
	Orthopyroxene	<5	<1	Anhedral to subhedral		
	Clinopyroxene	<5	<1	Anhedral to subhedral		
	Hornblende	<5	<2	Subhedral to euhedral		
	Opaque	<5	<1	Anhedral		
	Groundmass	50		Plag, bi, opaque, glass, cpx		
JL-AZU-006					Hypocrystalline & porphyritic	Andesite
	Plagioclase	20	<4	Anhedral to subhedral, lamellar & simple twinning, oscillatory zoning		
	Biotite	5	<4	Anhedral to subhedral		
	Olivine	<5	<2	Subhedral		
	Clinopyroxene	<5	<1	Anhedral		
	Orthopyroxene	<5	<1	Subhedral		
	Opaque	<5	<1	Anhedral		
	Groundmass	60		Plag, cpx, opx, opaques, glass		

Sample	Mineral	Modal %	Grain size (mm)	Description	Texture	Rock type
JL-AZU-007					Hypocrystalline & porphyritic	Andesite
	Plagioclase	25	<4	Anhedral to subhedral, lamellar & simple twinning, oscillatory zoning		
	Biotite	10	<3	Anhedral to subhedral		
	Orthopyroxene	5	<1	Anhedral to euhedral		
	Clinopyroxene	<5	<1	Subhedral,fractured xenolith		
	Opaques	<5	<1			
	Hornblende	<5	<2	Anhedral to subhedral		
	Groundmass	60		Plag, opx, and glass		
JL-AZU-008					Hypocrystalline & porphyritic	Andesite
	Plagioclase	25	<5	Anhedral to subhedral, lamellar & simple twinning, oscillatory zoning		
	Biotite	10	<5	Anhedral to subhedral		
	Orthopyroxene	5	<1	Anhedral to subhedral		
	Hornblende	<5	<1	Anhedral to subhedral		
	Groundmass	60		Plag, opx, bi, glass, opaques		
JL-AZU-009					Hypocrystalline & porphyritic	Andesite
	Plagioclase	20	<2	Anhedral to subhedral, lamellar & simple twinning, oscillatory zoning		
	Olivine	15	<4	Subhedral		
	Clinopyroxene	5	<2	Anhedral to subhedral		
	Biotite	<5	<2	Anhedral		
	Orthopyroxene	<5	<1	Anhedral to subhedral		
	Groundmass	60		Plag, cpx, glass		
JL-AZU-010					Hypocrystalline & porphyritic	Andesite
	Plagioclase	30	<3	Anhedral to euhedral, lamellar & simple twinning, oscillatory zoning		
	Clinopyroxene	5	<2	Anhedral to euhedral		
	Biotite	5	<2	Anhedral to subhedral		
	Orthopyroxene	<5	<1	Anhedral to subhedral		
	Groundmass	55		Plag, cpx, glass		

Sample	Mineral	Modal %	Grain size (mm)	Description	Texture	Rock type
JL-AZU-011					Hypocrystalline & porphyritic, glomerocrysts of cpx and opx	Andesite
	Plagioclase	25	<4	Anhedral to euhedral, lamellar & simple twinning, oscillatory zoning		
	Clinopyroxene	5	<1	Anhedral to subhedral		
	Olivine	5	<1	Anhedral to subhedral		
	Biotite	5	<1	Anhedral to subhedral		
	Orthopyroxene	5	<1	Anhedral to subhedral		
	Opaque	<5	<1	Anhedral		
	Groundmass	55		Plag, opx, cpx, glass		
JL-AZU-012					Hypocrystalline & porphyritic, layered	Dacite
	Plagioclase	30	<2	Anhedral to subhedral, lamellar & simple twinning, oscillatory zoning		
	Orthopyroxene	10	<1	Anhedral to subhedral		
	Biotite	<5	<1	Anhedral		
	Opaque	<5	<1	Anhedral		
	Groundmass	55		Alternating bands of glass and glass, opx & plag		

6 Results

In total 18 lava flows were sampled for study in this thesis. The 18 samples retrieved from Azufre were from fresh, apparently unaltered lava flows, which possibly resulted in a bias towards younger lavas and an underrepresentation of older lava flows, with the possibility that some were not sampled at all. The lava samples cluster on a TAS diagram along the boundaries between the andesite and trachyandesite, and dacite and trachyte fields. The data can be seen in Tables 3 and 4, and is plotted in Figure 4. Samples JL-AZU-004 and JL-AZU-012, of the first sample suite, are classified as a trachyte and dacite, with SiO_2 wt% of 65.66 and 65.35, respectively. The other 10 samples of the first suite of samples are classified as andesites, with SiO_2 wt% between 59.71 and 62.98. The second suite of samples all classify as andesites, with SiO_2 wt% between 60.47 and 63.19, with two outlying samples (AZU-17-002 and AZU-17-004) plotting in the trachyandesite field. All samples were analysed for major element, trace element, radiogenic and oxygen isotope compositions.

6.1 Major Elements

Major element data, as determined by XRF analysis, are presented in Table 3. Results have not been recalculated to 100% anyhdrous. Azufre samples have high SiO_2 (59.71 - 65.66 wt.%), moderate alkali ($Na_2O + K_2O$: 5.97 - 7.53 wt.%) and TiO_2 (0.5 - 0.8 wt.%), and low MgO (1.36 - 3.65 wt.%) and CaO (3.48 - 6.22 wt.%) contents. $Na_2O + K_2O$ shows a positive correlation with SiO_2, with a correlation coefficient (r) = 0.87 . This trend is comparable to those of the SPLVC and can be seen in Figure 4. Compositional trends for Fe_2O_3, CaO, MgO, and TiO_2 show a negative correlation with SiO_2, with Pearson's r values = -0.64, -0.68, -0.69, and -0.5 respectively (Figure 5).

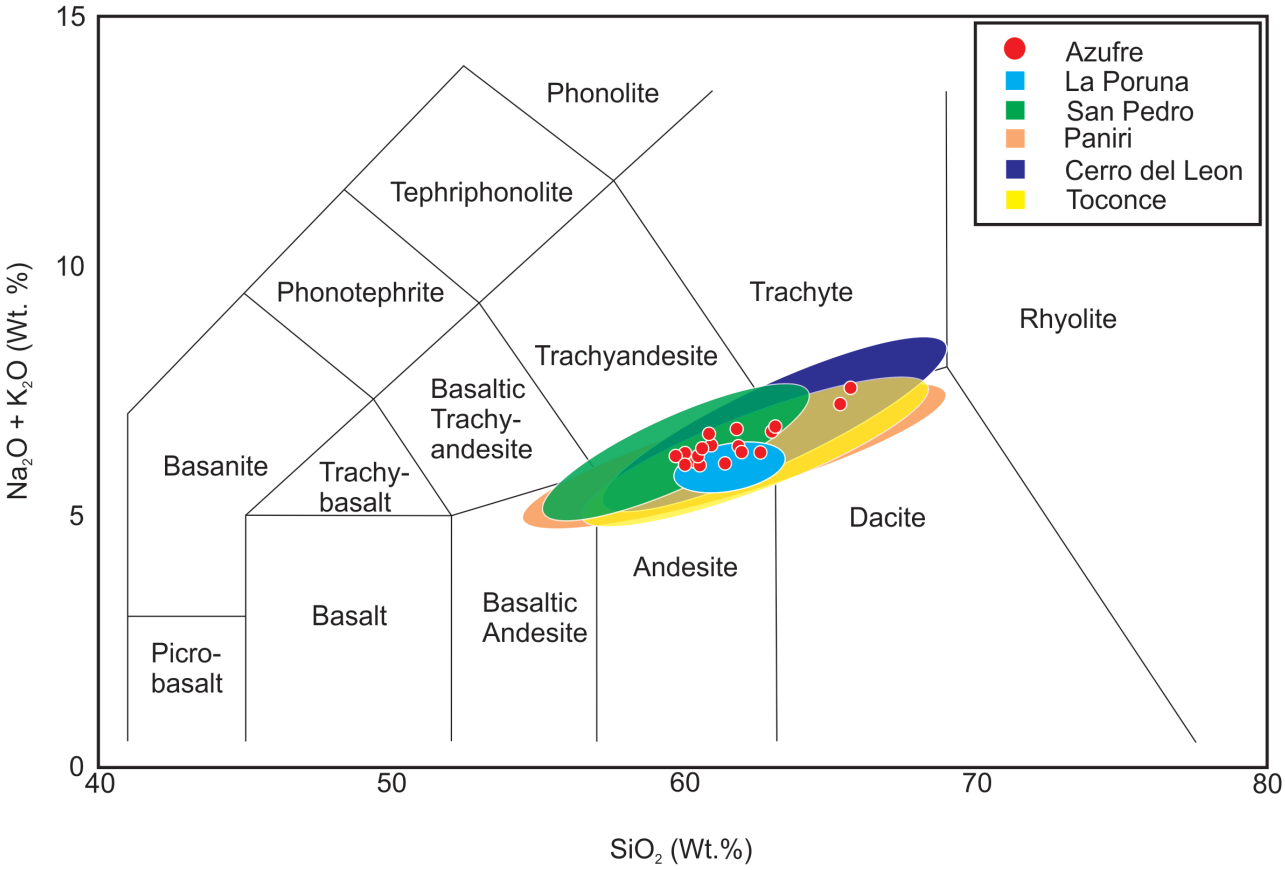

Figure 4: Total-Alkali vs. Silica (TAS) diagram for sampled lavas from Azufre (red) and the San Pedro-Linzor chain (after Godoy et al. (2014), coloured fields). Both sets of samples show well-defined sub-alkaline trends, with Azufre lavas varying from andesitic to dacitic in composition.

6.2 Trace Elements

Trace element concentrations of the collected samples were obtained by XRF and Quadrupole-ICP-MS analysis, the full results are displayed in Table 3 and 4 respectively. Trace element data collected from ICP-MS and XRF analysis are in good agreement. ICP-MS analysed trace element and REE data have been normalised to primitive mantle and chondritic values respectively (after Sun & McDonough (1989)) and displayed in Figure 6. Incompatible trace element patterns normalised to the primitive mantle composition show relative enrichment in Rb, Th, U, Pb and Sr, and depletion in Nb, Ta, Zr and Eu. This negative Eu anomaly is visible in the chondrite normalised REE patterns, with Eu anomaly values (Eu^*) of 17.79 to 27.79, where Eu^* is defined as: $(Eu^* = 10^{(\frac{log(Sm_N)+log(Gd_N)}{2})} \sim 0.7)$.

The elements Sr and Cr show a negative correlation with SiO_2. Ni appears to show a negative correlation with SiO_2, however many of the values are <5 ppm, and therefore below the detection limit of the XRF, resulting in a plot that is not very reliable. Ba, Rb and Zr show positive correlations with SiO_2. Most of the trace element correlations are not as strong as the major element correlations presented earlier. The sampled lava flows show Ni <5 ppm, Rb 80 - 210

ppm, Cr <65 (bar one outlier), and Mg# <35.

Azufre lavas are enriched in fluid-mobile large ion lithophile elements (LILE), relative to high field strength elements (HFSE), and are enriched in light rare earth elements (LREE) relative to heavy rare earth elements (HREE). These relationships are shown in Figure 6 where the LILE and LREE on the left display high concentrations, while the HFSE and HREE on the right display low concentrations.

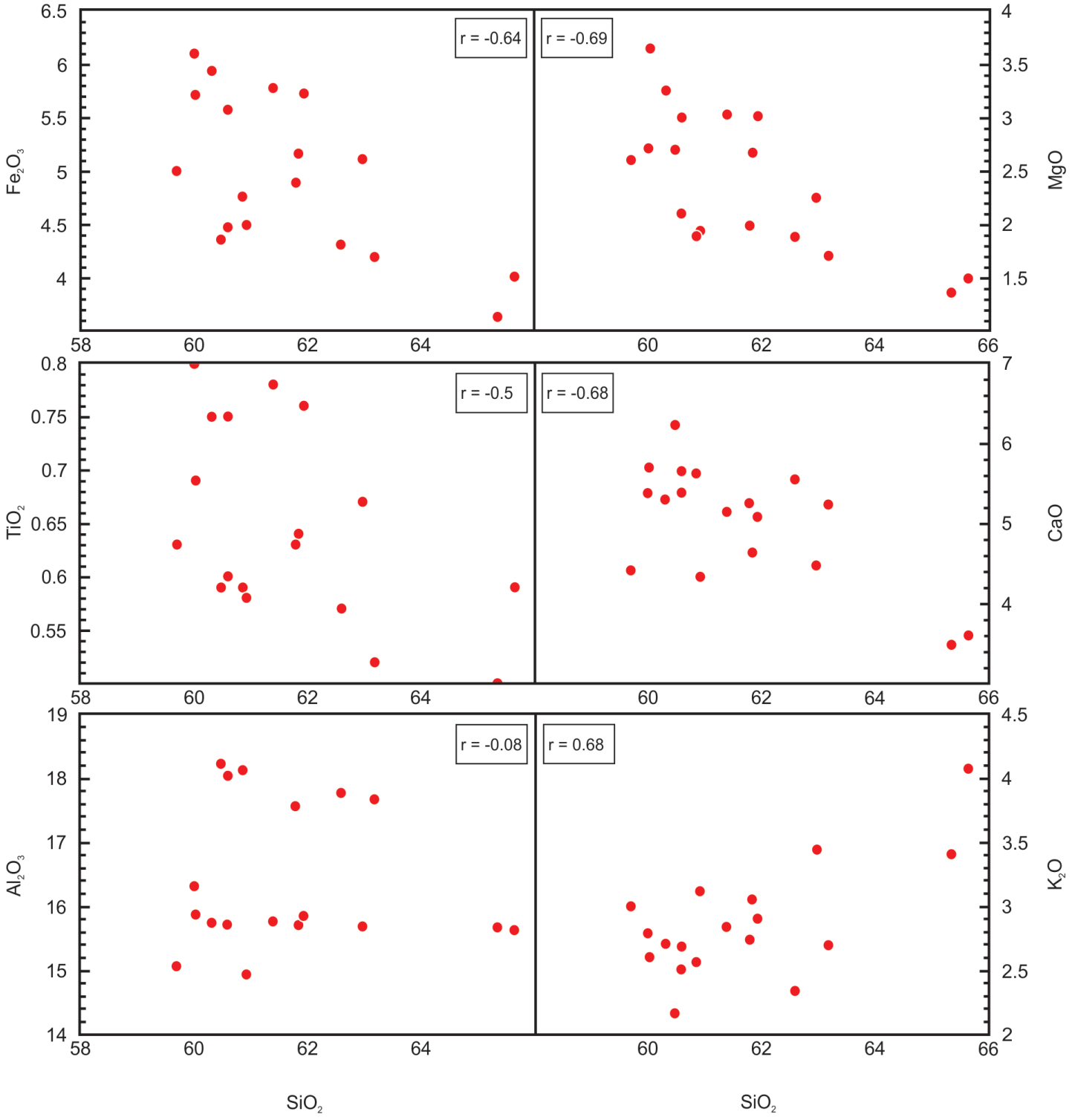

Figure 5: Major oxides vs. SiO_2 for sampled lavas from Azufre. Decreases of Fe_2O_3, MgO, TiO_2, CaO, and Al_2O_3, and an increase in K_2O, with increasing SiO_2 can be observed.

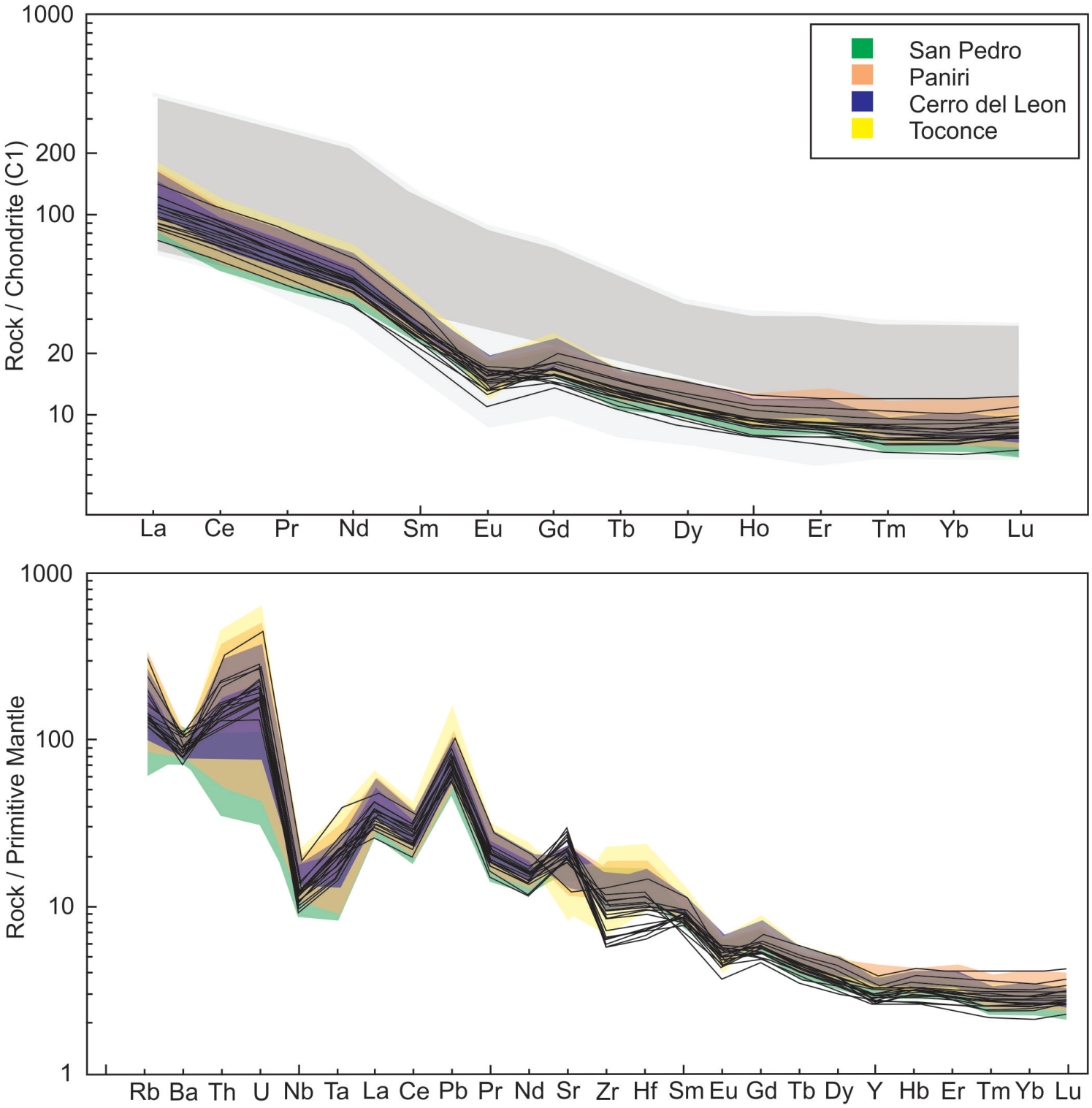

Figure 6: a) REE normalized to chondritic values. Gray area represents normalized composition of lavas erupted in the Central Andes (after (Mamani et al., 2010)) and b) Trace elements normalized to primitive mantle diagrams (after (Sun & McDonough, 1989)) for Azufre lavas

Table 3: Geochemical results for Azufre lava samples from XRF

Major Oxide (wt%)	JL-AZU-001	JL-AZU-002	JL-AZU-003	JL-AZU-004	JL-AZU-005	JL-AZU-006	JL-AZU-007	JL-AZU-008	JL-AZU-009
SiO_2	60.6	60.9	60.0	65.7	63.0	60.3	62.0	61.4	60.0
TiO_2	0.75	0.58	0.80	0.59	0.67	0.75	0.76	0.78	0.69
Al_2O_3	15.7	14.9	16.3	15.6	15.7	15.7	15.8	15.8	15.9
Fe_2O_3	5.57	4.49	6.10	4.01	5.11	5.93	5.72	5.77	5.71
MnO	0.09	0.08	0.10	0.07	0.08	0.09	0.09	0.09	0.09
MgO	3.00	1.93	2.71	1.50	2.25	3.25	3.01	3.02	3.65
CaO	5.37	4.32	5.37	3.59	4.48	5.30	5.07	5.15	5.69
Na_2O	3.32	3.28	3.43	3.46	3.22	3.35	3.36	3.19	3.37
K_2O	2.68	3.11	2.79	4.07	3.43	2.70	2.90	2.84	2.60
P_2O_5	0.21	0.23	0.24	0.17	0.21	0.20	0.20	0.21	0.17
LOI	1.56	1.53	0.69	0.60	1.40	0.96	0.92	1.26	0.92
Total	99.2	99.4	98.7	99.8	99.8	98.9	100.0	99.8	99.0
Minor Elements (ppm)									
Ba	726	708	755	675	766	724	729	739	653
Cr	56	13	12	16	11	65	53	55	104
Ni	<5	<5	<5	<5	<5	5	<5	<5	8
Rb	101	151	114	210	149	102	110	100	101
Sr	500	429	481	324	424	495	479	485	459
Zr	169	154	173	233	185	171	166	179	151
Zn	72	57	77	47	66	73	72	75	70
Cu	16	13	14	12	16	15	10	14	15
Mo	<5	<5	<5	<5	<5	<5	<5	<5	<5
Nb	12	13	13	18	14	13	13	13	11
Y	18	20	24	27	20	19	14	24	18
U	<5	<5	<5	11<5	<5	<5	<5	<5	
Th	11	21	14	38	21	12	12	11	11
Pb	14	17	16	22	19	15	15	14	15
Co	8	5	9	<5	<5	13	8	9	13
Mn	684	570	740	446	628	698	662	663	701
V	122	103	140	67	104	128	125	123	134
F	581	650	650	444	517	541	496	496	369
S	1649	747	482	355	365	463	365	465	426
Cl	266	463	280	117	270	332	291	316	281
Sc	17	12	17	10	14	18	15	16	18

Major Oxide (wt%)	JL-AZU-010	JL-AZU-011	JL-AZU-012	AZU-17-001	AZU-17-002	AZU-17-004	AZU-17-005	AZU-17-008	AZU-17-011
SiO_2	61.9	59.7	65.4	62.6	61.8	60.9	63.2	60.5	60.6
TiO_2	0.64	0.63	0.50	0.57	0.63	0.59	0.52	0.59	0.60
Al_2O_3	15.7	15.1	15.7	17.8	17.6	18.1	17.7	18.2	18.0
Fe_2O_3	5.16	4.99	3.63	4.31	4.88	4.76	4.19	4.36	4.47
MnO	0.09	0.08	0.07	0.06	0.07	0.07	0.07	0.07	0.06
MgO	2.67	2.59	1.36	1.88	1.98	1.88	1.70	2.70	2.09
CaO	4.62	4.41	3.48	5.54	5.24	5.61	5.23	6.22	5.64
Na_2O	3.31	3.20	3.81	3.92	3.99	4.05	4.08	4.00	3.78
K_2O	3.05	3.00	3.40	2.34	2.73	2.56	2.69	2.16	2.51
P_2O_5	0.21	0.17	0.15	0.15	0.18	0.18	0.14	0.17	0.15
LOI	1.30	1.38	1.18	0.30	0.13	0.44	-0.07	0.45	1.08
Total	98.9	99.7	98.7	99.5	99.2	99.1	99.4	99.5	99.1
Minor Elements (ppm)									
Zn	66	65	53	55	56	55	46	55	59
Cu	10	9	9	9	16	14	20	16	14
Ni	<5	<5	<5	-3	-3	-5	-3	-2	1
Mo	<5	<5	<5	<5	<5	<5	<5	<5	<5
Nb	13	13	13	12	14	14	12	10	12
Zr	182	182	169	161	178	190	170	149	164
Y	24	21	14	19	21	23	19	17	20
Sr	450	450	434	580	553	594	553	575	581
Rb	120	125	136	82	124	109	125	83	92
U	<5	<5	<5	<5	<5	<5	<5	<5	<5
Th	14	15	13	10	16	13	15	10	11
Pb	16	17	18	13	15	15	15	12	11
Co	9	9	<5	<5	7	<5	<5	5	5
Mn	619	606	480	486	531	527	486	570	521
Cr	64	62	18	41	22	23	30	55	51
V	111	108	76	87	94	91	83	104	88
F	478	453	339	490	545	555	408	508	476
S	509	373	333	266	279	272	284	585	270
Cl	294	322	312	167	189	249	136	165	173
Sc	14	14	9	12	12	14	12	16	14
Ba	752	742	827	703	769	721	648	610	684

Table 4: Trace elements for Azufre lava samples from ICP-MS

Trace Element	JL-AZU-001	JL-AZU-002	JL-AZU-003	JL-AZU-004	JL-AZU-005	JL-AZU-006	JL-AZU-007	JL-AZU-008	JL-AZU-009
Li	27.4	38.6	31.5	38.9	47.8	25.6	26.3	26.0	22.2
Sc	11.6	9.91	14.2	7.85	11.6	12.8	11.6	11.5	13.8
V	107	94.9	145	65.7	97.9	112	109	109	114
Cr	52.4	16.1	15.2	14.5	14.0	55.0	51.5	52.2	104
Co	9.84	6.45	9.17	5.15	8.06	10.4	9.98	9.73	11.8
Ni	17.6	8.60	11.2	13.9	10.7	21.5	18.8	17.9	26.9
Cu	22.1	17.4	19.1	16.0	21.0	18.9	14.3	19.3	20.1
Zn	89.4	75.4	94.0	68.0	88.4	86.8	88.6	93.5	79.2
Rb	92.0	129	112	215	182	91.8	89.1	94.9	86.2
Sr	512	438	520	281	497	502	456	516	448
Y	12.7	13.6	16.4	19.1	15.9	13.1	13.0	13.7	13.5
Zr	106	69.3	121	161	105	104	109	116	126
Nb	8.91	10.4	9.67	14.8	10.8	8.51	9.24	9.36	8.23
Ba	745	640	768	640	828	661	683	688	642
La	23.1	26.5	25.5	35.8	31.7	22.2	23.3	24.2	19.0
Ce	47.9	53.9	52.8	69.8	60.4	45.3	48.8	50.1	38.6
Pr	5.60	5.96	6.16	8.34	7.10	5.33	5.62	5.87	4.51
Nd	21.3	21.8	23.3	29.6	26.1	20.3	21.5	22.6	17.2
Sm	4.05	4.04	4.52	5.46	4.70	3.95	4.17	4.41	3.44
Eu	0.90	0.81	0.98	0.85	0.92	0.88	0.91	0.98	0.82
Tb	0.49	0.49	0.58	0.67	0.59	0.49	0.51	0.54	0.44
Gd	3.41	3.41	3.91	4.44	3.94	3.33	3.50	3.67	3.18
Dy	2.79	2.87	3.40	3.91	3.36	2.80	2.90	3.06	2.63
Ho	0.53	0.56	0.67	0.76	0.64	0.54	0.54	0.56	0.48
Er	1.43	1.57	1.89	2.15	1.77	1.50	1.49	1.51	1.36
Tm	0.20	0.24	0.28	0.33	0.26	0.20	0.21	0.22	0.19
Yb	1.35	1.55	1.79	2.18	1.68	1.38	1.39	1.39	1.31
Lu	0.20	0.24	0.29	0.34	0.27	0.22	0.21	0.21	0.21
Hf	3.10	2.35	3.47	4.96	3.22	3.03	3.22	3.39	3.60
Ta	0.87	1.10	0.89	1.73	1.05	0.73	0.79	0.80	0.87
Pb	11.9	15.3	13.2	20.6	17.7	12.1	12.8	12.6	11.7
Th	11.2	18.8	13.6	30.5	20.6	11.0	12.0	11.4	12.0
U	3.74	5.98	4.10	10.2	6.07	3.56	3.97	3.57	2.99

Trace Elements	JL-AZU-010	JL-AZU-011	JL-AZU-012	AZU-17-001	AZU-17-002	AZU-17-004	AZU-17-005	AZU-17-008	AZU-17-011
Li	24.9	25.0	30.5	26.8	33.8	33.9	31.9	26.0	27.4
Sc	9.80	10.1	6.04	8.61	8.32	8.67	10.2	15.7	9.59
V	99.9	100	65.4	79.6	101	75.9	86.6	105	104
Cr	65.9	64.0	18.0	37.6	22.4	14.9	32.6	66.2	45.2
Co	9.03	8.78	4.16	6.38	6.59	5.27	7.05	8.27	9.45
Ni	19.0	16.7	6.99	7.99	6.82	6.20	11.9	10.0	35.2
Cu	13.8	111	11.5	19.3	26.7	21.5	34.1	29.3	22.9
Zn	79.5	80.3	62.2	68.9	72.9	63.7	66.9	75.3	80.1
Rb	94.9	101	117	89.6	111	105	148	100	87.7
Sr	424	431	458	632	504	608	641	692	574
Y	16.0	15.9	13.8	13.1	14.5	15.0	15.8	15.0	14.6
Zr	134	135	147	81.7	78.6	72.6	77.8	70.3	88.9
Nb	9.71	9.81	9.78	7.59	9.08	8.68	8.82	7.19	7.88
Ba	796	710	878	620	558	622	629	598	597
La	23.3	22.5	21.9	28.3	29.0	29.4	31.4	25.7	29.0
Ce	46.9	47.0	43.8	53.0	59.8	57.9	59.9	48.0	55.9
Pr	5.63	5.42	4.94	5.96	6.49	6.47	6.75	5.57	6.44
Nd	21.2	20.6	17.9	21.7	23.9	24.0	24.2	20.7	24.1
Sm	4.00	3.91	3.29	3.80	4.24	4.41	4.32	3.94	4.29
Eu	0.81	0.80	0.69	1.02	0.94	1.06	1.07	1.05	1.05
Tb	0.53	0.52	0.42	0.46	0.49	0.51	0.53	0.49	0.51
Gd	3.75	3.72	3.02	3.24	3.50	3.56	3.62	3.26	3.54
Dy	2.99	2.93	2.42	2.52	2.81	2.94	3.00	2.83	2.82
Ho	0.58	0.58	0.48	0.48	0.53	0.58	0.57	0.57	0.54
Er	1.60	1.58	1.39	1.29	1.47	1.56	1.61	1.63	1.49
Tm	0.24	0.23	0.21	0.18	0.21	0.22	0.23	0.24	0.19
Yb	1.52	1.49	1.37	1.15	1.37	1.45	1.57	1.56	1.29
Lu	0.26	0.24	0.22	0.19	0.22	0.22	0.25	0.24	0.21
Hf	3.85	3.89	4.19	2.41	2.53	2.35	2.45	2.15	2.62
Ta	0.92	0.90	1.00	0.68	0.87	0.82	0.93	0.65	0.67
Pb	13.7	13.4	15.8	15.6	14.3	14.8	16.6	13.0	11.3
Th	15.5	15.4	13.9	13.3	14.2	15.4	21.1	14.4	12.4
U	4.57	4.50	5.30	4.96	5.27	4.92	6.53	4.09	4.06

6.3 Radiogenic and Stable Isotopes

All 18 samples collected from Azufre were analysed for Nd, Sr, and O isotopes.

Azufre lavas have $^{87}Sr/^{86}Sr$ ratios between 0.7067 and 0.7075. These isotope ratios have a similar range to those for La Poruna, San Pedro and Paniri lavas obtained by Godoy et al. (2014, 2017), located in the nearby San Pedro-Linzor chain, and are relatively high in comparison to other lavas of the Central Andes. Non-APVC lavas have $^{87}Sr/^{86}Sr$ values ranging from 0.703 to approximately 0.706 (Godoy et al., 2014; Mamani et al., 2008). The $^{87}Sr/^{86}Sr$ ratios tend to a weak positive correlation with SiO_2 wt%. Full results are displayed in Table 5.

Azufre lavas have $^{143}Nd/^{144}Nd$ ratios between 0.5123 and 0.5124 and εNd of -5.29 to -6.7, which are comparable to those of the San Pedro-Linzor chain and relatively low when compared to other Central Andes lavas. Non-APVC lavas have εNd values from -4 to 5 (Godoy et al., 2014; Mamani et al., 2008). The $^{143}Nd/^{144}Nd$ ratios show no correlation with SiO_2 wt%. Full results are displayed in Table 5.

Mineral separate $\delta\ ^{18}O$ values were obtained for quartz from the Azufre samples. Of all the crystals picked there may have been several that; (a) were in fact plagioclase and not quartz, as they can appear very similar, and (b) were not primary crystals but rather secondary quartz that formed as veins or amygdales. Azufre lavas have $\delta\ ^{18}O$ that range between 7.85‰and 9.72‰. Several samples were analysed twice, either due to space limitations on the laser line or due to samples of inferior quality being picked for the initial run. The outlier value recorded for sample AZU-17-011 was interpreted as having come from an amygdale (11.95‰). Full results are displayed in Table 5

6.3.1 Comparison of Stable and Radiogenic Isotopes

Whole-rock $\delta\ ^{18}O$ values are plotted against ε_{Nd} on Figure 7 (calculated to present day CHUR value of 0.512638 (Fowler, 2005)) and $^{87}Sr/^{86}Sr$, and shows two distinct trends. When the outlying sample is removed the correlation for ε_{Nd} changes from 0.015 to 0.43. The range of ε_{Nd} for the collected samples is -6.701 to -5.293 and the average ε_{Nd} is -5.989. This average value is considerably below that of the depleted mantle's $\sim$10.

Table 5: Isotope Ratios

Sample	$^{87}Sr/^{86}Sr$	$^{143}Nd/^{144}Nd$	δ ^{18}O Quartz	δ ^{18}O Quartz Repeat	
JL-AZU-001	0.707152	0.512334	8.01[1]	8.91	
JL-AZU-002	0.706984	0.512325	9.22	8.13	
JL-AZU-003	0.706881	0.512321	8.25		
JL-AZU-004	0.707460	0.512315	9.72	9.37	
JL-AZU-005	0.706917	0.512328			
JL-AZU-006	0.706958	0.512340	8.53		
JL-AZU-007	0.707142	0.512323	8.28		
JL-AZU-008	0.707321	0.512294	7.85	7.93	
JL-AZU-009	0.706680	0.512367	8.99		
JL-AZU-010	0.706798	0.512335			
JL-AZU-011	0.706856	0.512353	9.36		
JL-AZU-012	0.706730	0.512356			
AZU-17-001	0.707261	0.512327	9.79	8.99	9.57
AZU-17-002	0.707117	0.512316	8.15		
AZU-17-004	0.707145	0.512323	8.30	8.41	
AZU-17-005	0.706994	0.512347		8.64	
AZU-17-008	0.706984	0.512338	8.25	8.60	8.52
AZU-17-011	0.707302	0.512315	14.58	9.31	

[1] δ ^{18}O values are on individual crystals, and as such the differences in δ ^{18}O value may not be down to analytical error.

7 Discussion

7.1 General Classification

Lavas from Azufre show variation, on a TAS diagram (Fig. 4), from andesite to dacite/trachyte. The Azufre lavas display a positive correlation of r = 0.87, which is consistent with the lavas of the SPLVC, indicating that alkali content increases to an almost linear degree with magmatic evolution. Like the lavas of the San Pedro — Linzor volcanic chain (SPLVC), Azufre lava major oxides display trends, the values of which place them within the high-K, calc-alkaline series as described by Rickwood (1989). Trace element values for Azufre are similar to those of the SPLVC, and are common for subduction related arc magmatism. Likewise REE patterns of Azufre are similar to those of the SPLVC (Fig. 6), displaying a flatter pattern (low LREE/HREE) than most other erupted products in the central Andes. These low observed LREE/HREE ratios indicate that melting occurred under conditions where garnet is not a stable phase. Garnet is only stable under high pressure conditions, which results in highly depleted HREE signatures, due to HREEs being compatible in garnet. Lavas from Azufre display particularly low Eu/Eu* ratios (Fig. 7). These low Eu/Eu* ratios as well as a negative correlation between Eu/Eu* and SiO_2 indicate a strong role for plagioclase fractionation during differentiation. Plagioclase has been experimentally shown to only be stable under low pressure conditions (<10k bar $\approx$ 40km). This suggested important role for plagioclase fractionation combined with the absence of a garnet signature are indicators that magmatic evolution occurred under shallow crustal conditions (Taylor & McLennan, 1988).

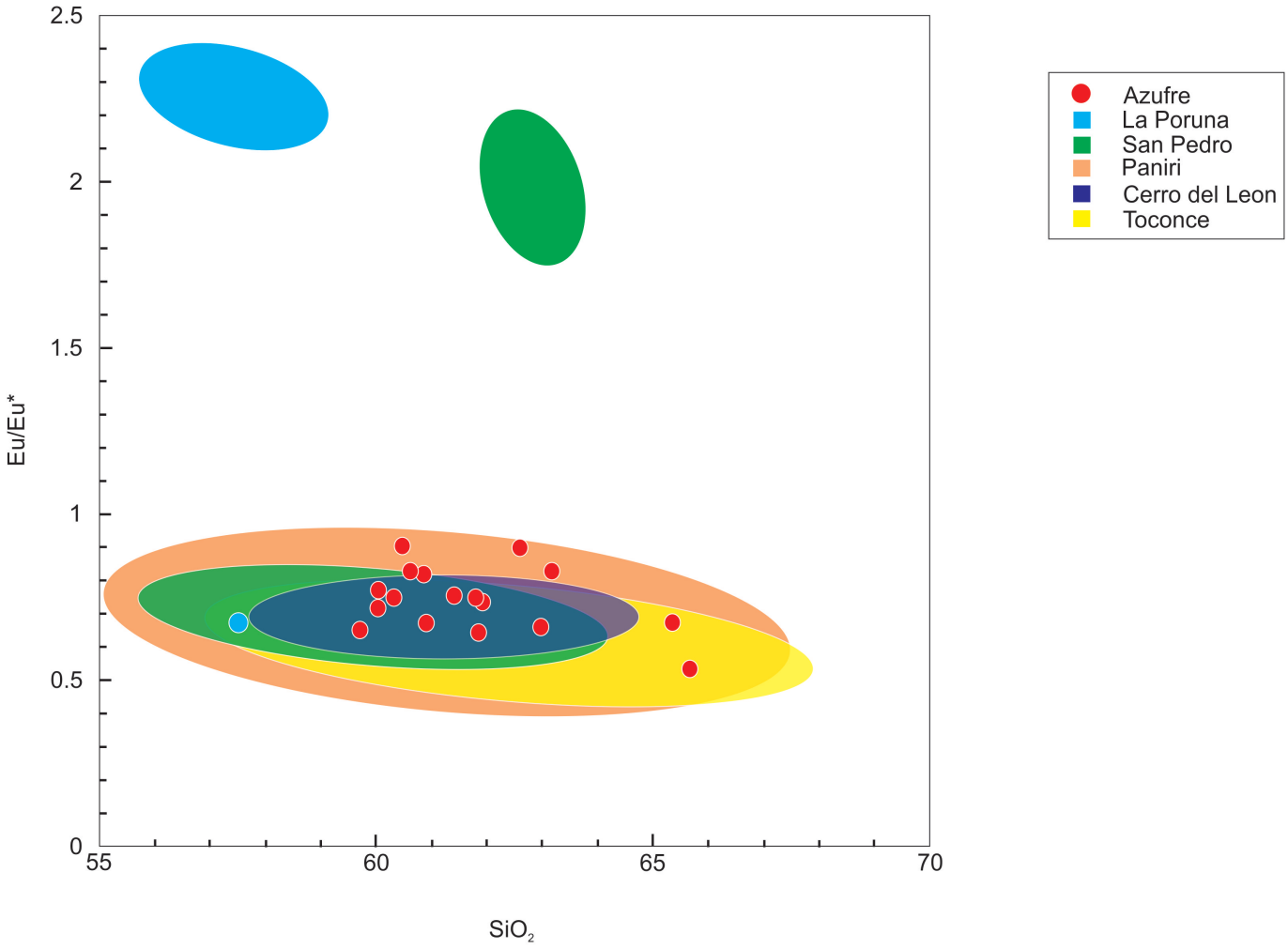

Figure 7: SiO_2 vs. Eu/Eu* plot for analysed samples from Azufre and the SPLVC. La Poruna and San Pedro data plots both in the same region as Azufre and the other volcanoes of the SPLVC, as well as as outliers with higher Eu/Eu* values.

7.2 Fractional Crystallisation

Fractional crystallisation was modelled using major and trace element data. The major element data were modelled graphically on variation diagrams and by using a least squares model, performed on an Excel spreadsheet, and the trace element data were modelled using Rayleigh's Law of Fractionation.

Due to the lack of a definite parent magma for the Azufre lavas a lava sample from nearby La Poruna (POR 10 01), from Godoy et al. (2014), was chosen as a representative parent magma, and was used for the modelling of select Azufre lavas. La Poruna was chosen as the parent magma as it is located relatively close to Azufre and has lavas which are much more mafic in

their composition than Azufre, or any of the other surrounding volcanoes. Previous studies have used other primitive samples, however those are all sourced considerably far from the study area and where therefore excluded in favour of La Poruna.

7.2.1 Major Element Modelling

Major element modelling was performed by least squares modelling in Microsoft Excel. Table 6 shows the outputs for fractional crystallisation from POR 10 01 (parent) to the daughter samples; JLA-AZU-001, JL-AZU-004, JLA-AZU-006, AND JL-AZU-008.

Table 6 shows that for JL-AZU-001 and JL-AZU-004 the amount of crystal fractionation is 44% and 67% respectively, and that for JL-AZU-006 and JL-AZU-008 the amount of fractionation is 45% and 42% respectively. The minerals that have been modelled fractionating are plagioclase, clinopyroxene, orthopyroxene, Ti-magnetite, and olivine. The main fractionating phase is plagioclase, with clinopyroxene and orthopyroxene as the second most abundant phases (dependant on the sample), and with olivine and Ti-magnetite as minor fractionating phases.

Representative major element variation diagrams (Figures 8 and 9) plotting whole-rock data and mineral phase compositions, indicated to be fractionating by modelling, were also produced. The extrapolation of the evolution trend to the combination of modelled phases fractionated shows an observable decrease in major elements with increasing silica, suggesting that there is indeed evolution by fractional crystallisation, which supports the results of the least squares modelling.

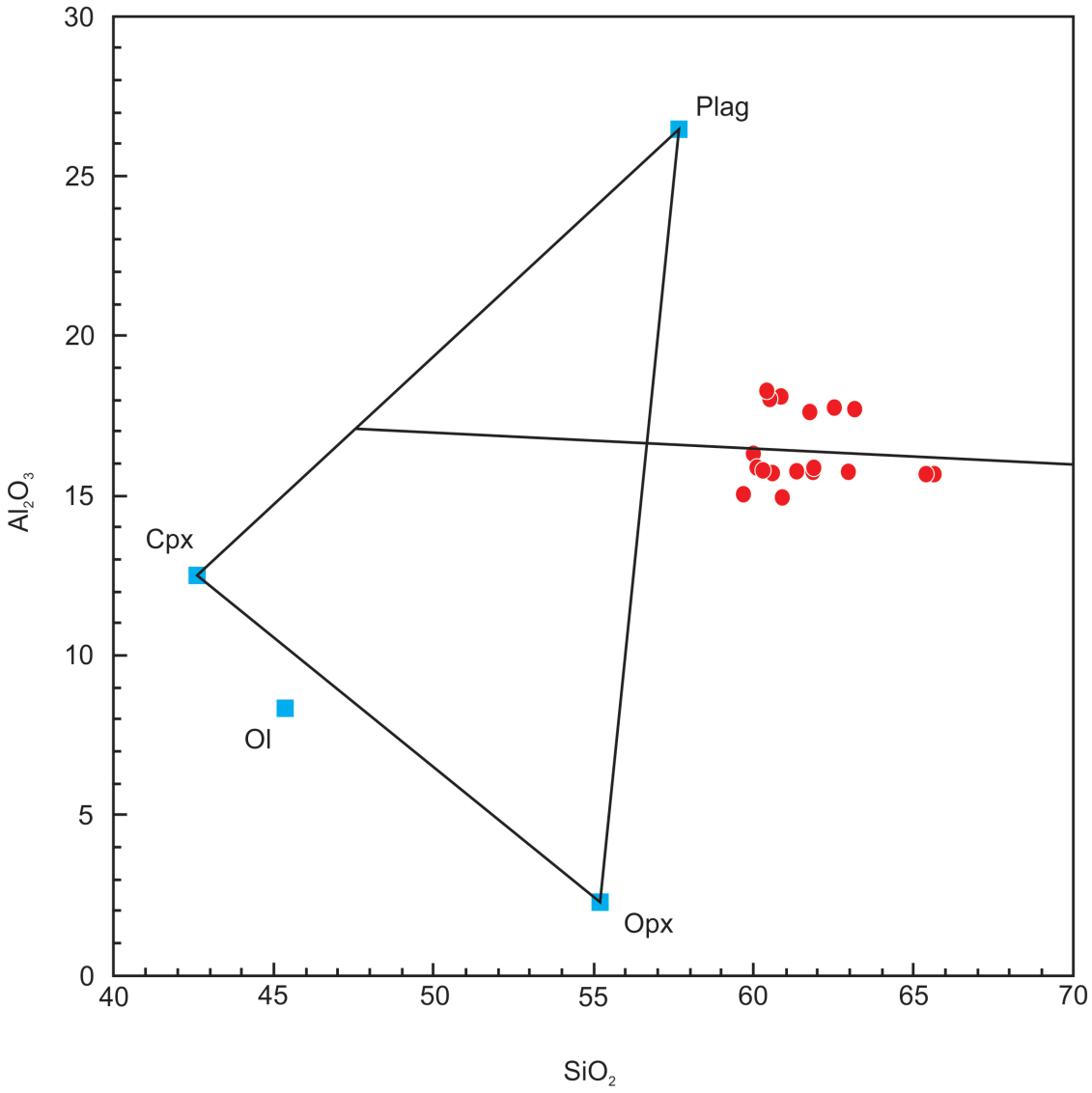

Figure 8: Variation diagram plotting SiO_2 vs Al_2O_3, where the fractionating assemblage plots variably along the line of best fit (but within the triangular field)

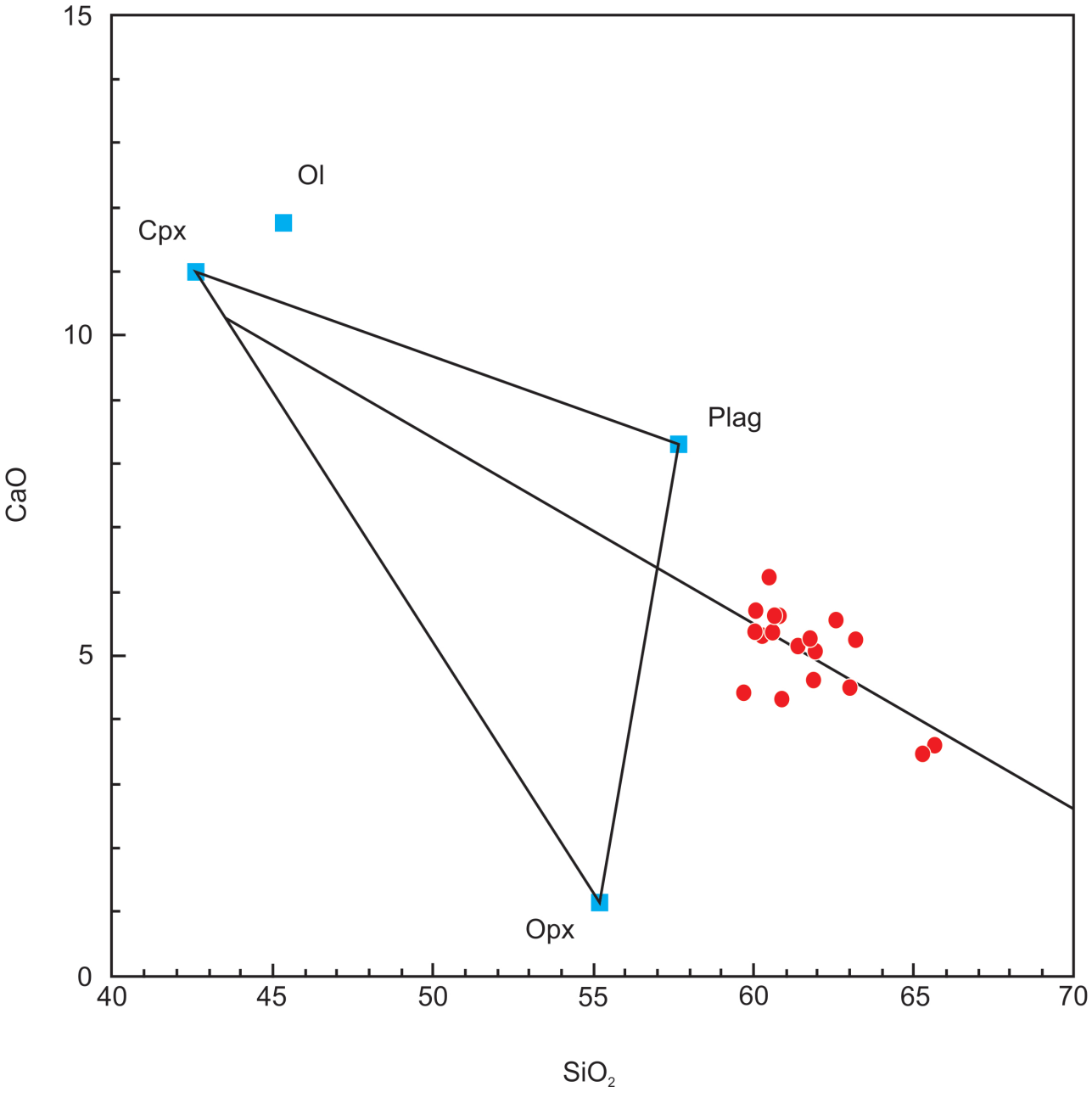

Figure 9: Variation diagram plotting SiO_2 vs CaO, where the fractionating assemblage plots variably along the line of best fit (but within the triangular field)

Table 6: Model Results

	Observed POR 10 01	Calculated POR 10 01	Difference	JL-AZU-001	Mix	Wt.%
SiO_2	57.52	57.53	-0.015	60.59	JL-AZU-001	56[2]
TiO_2	0.78	0.60	0.179	0.75	Olivine	0.331
Al_2O_3	16.21	16.20	0.006	15.69	Clinopyroxene	5.83
FeO	6.24	6.25	-0.014	5.57	Plagioclase	27
MnO	0.11	0.09	0.022	0.09	Fe-Ti Oxides	1.99
MgO	5.29	5.26	0.029	3.00	Orthopyroxene	8.71
CaO	6.39	6.38	0.012	5.37		
Na_2O	3.75	3.67	0.084	3.32	Total	100
K_2O	1.79	1.67	0.118	2.68		
Sum of Squares			0.05			

	Observed POR 10 01	Calculated POR 10 01	Difference	JL-AZU-004	Mix	Wt.%
SiO_2	57.52	57.53	-0.012	65.66	JL-AZU-004	33
TiO_2	0.78	0.46	0.316	0.59	Olivine	1.60
Al_2O_3	16.21	16.18	0.034	15.61	Clinopyroxene	9.44
FeO	6.24	6.28	-0.037	4.01	Plagioclase	41
MnO	0.11	0.15	-0.037	0.07	Fe-Ti Oxides	1.89
MgO	5.29	5.24	0.051	1.50	Orthopyroxene	13.1
CaO	6.39	6.40	-0.01	3.59		
Na_2O	3.75	3.78	-0.028	3.46	Total	100
K_2O	1.79	1.73	0.060	4.07		
Sum of Squares			0.11			

[2] % liquid remaining

	Observed POR 10 01	Calculated POR 10 01	Difference	JL-AZU-006	Mix	Wt.%
SiO_2	57.52	57.56	-0.036	60.32	JL-AZU-006	55
TiO_2	0.78	0.67	0.093	0.75	Olivine	4.76
Al_2O_3	16.21	16.20	-0.069	15.74	Clinopyroxene	11.0
FeO	6.24	6.27	-0.057	5.93	Plagioclase	27
MnO	0.11	0.09	0.025	0.09	Fe-Ti Oxides	2.02
MgO	5.29	5.29	-0.035	3.25	Orthopyroxene	0
CaO	6.39	6.39	-0.043	5.30		
Na_2O	3.75	3.78	0.074	3.35	Total	100
K_2O	1.79	1.76	-0.072	2.70		
Sum of Squares			0.02			

	Observed POR 10 01	Calculated POR 10 01	Difference	JL-AZU-008	Mix	Wt.%
SiO_2	57.53	57.56	-0.039	61.41	JL-AZU-008	52
TiO_2	0.60	0.75	0.034	0.78	Olivine	0.011
Al_2O_3	16.20	16.25	-0.040	15.76	Clinopyroxene	16.1
FeO	6.25	6.29	-0.046	5.77	Plagioclase	22
MnO	0.09	0.16	-0.045	0.09	Fe-Ti oxides	0.078
MgO	5.26	5.32	-0.026	3.02	Orthopyroxene	3.86
CaO	6.38	6.44	-0.046	5.15		
Na_2O	3.67	3.73	0.017	3.19	Total	100
K_2O	1.67	1.83	-0.035	2.84		
Sum of Squares			0.01			

Table 7: Mineral compositions from JL-AZU-006 used in model (data for all samples provided in Appendix)

Mineral Sample	SiO_2	TiO_2	Al_2O_3	FeO	MnO	MgO	CaO	Na_2O	K_2O	Total
AZU-006-PLG3-R1	59.5	0.039	25.8	0.258	0.036	0.006	7.06	7.07	0.693	100
AZU-006-OL1-C1	39.6	0.00	0.00	14.6	0.18	44.9	0.12			99.5
AZU-006-CPX2-C1	57.2	0.449	4.64	5.63	0.144	12.1	14.1	0.263	0.561	95.1
AZU-006-CPX3-R1	54.4	0.184	2.28	10.9	0.179	30.9	1.25	0.038	0.012	101
AZU-006-MAG3		9.66	2.03	79.0		1.16				91.9

7.2.2 Trace Element Modelling

The evolution of Azufre lavas has also been modelled using trace element data. For this modelling La Poruna is continued to be treated as the parent magma for Azufre lavas. For this modelling the amount of fractionation was calculated using major elements, and partition coefficients, from the Geochemical Earth Reference Model (EarthRef.org, 2018). The calculated values are compared to the actual trace element concentration in the Azufre samples. The modelling for this section was performed using the Rayleigh Fractionation Law:

$$\frac{Cl}{Co} = F^{\bar{D}-1} \tag{1}$$

$$\bar{D} = \sum_{i=1}^{n} D_i W_i \tag{2}$$

Where:
Cl = concentration of element in liquid
Co = concentration of element in initial liquid
F = weight fraction of liquid remaining
$\bar{\text{D}}$ = bulk partition coefficient
D = mineral/melt partition coefficient
W = weight fraction of mineral in extract

Samples JL-AZU-001, JL-AZU-006, and JL-AZU-008 show very similar values for all their calculated trace element data. JL-AZU-004 has significantly different values to the other three samples, and this is attributed to the far lower degree of fractionation (67 wt.% vs $\sim$ 45 wt.%).

Tables 8 and 9 show that calculated values for U, Nb, Zr, Y, and La are all approximately double those of the actual values, for the three similar samples whereas for JL-AZU-004 it is only the calculated values for Nb, Zr, and La that are approximately double those of the actual values. The calculated values for Ba, Sr, Eu, Yb, and Ni are approximately the same as the actual values for samples JL-AZU-001, JL-AZU-006, and JL-AZU-008 and for sample JL-AZU-004 U, Ba, Eu, Yb and Ni have values that are approximately the same. For samples JL-AZU-001, JL-AZU-006, and JL-AZU-008 Rb is approximately 10 ppm lower than the actual value and approximately 15 ppm lower for JL-AZU-004.

Table 8: Model Results

	JL-AZU-001	wt.% 55.7		Mineral Kd's					
Sample	POR 10 01	JL - AZU - 001	Cl Calculated	Plagioclase	Clinopyroxene	Magnetite	Olivine	Orthopyroxene	Bulk D
U	3.72	3.74	6.63	0.34	0.04	0	0.00	0.02	0.22
Ba	601	745	748	1	0.03	0	0.01	0.01	0.63
Nb	13.0	8.91	17.1	0.05	0.01	10	0.01	0.27	0.53
Zr	137	106	213	0.05	1.11	0.71	0.14	0.18	0.24
Y	16.9	12.7	23.5	0.2	1	0.2	0.01	0.54	0.37
Sr	560	512	513	1.83	0.06	0	0.01	0.04	1.15
Rb	46	92	82.2	0.01	0.00	0	0.00	0.01	0.01
La	37.1	23.1	53.2	0.28	0.19	3	0.01	0.26	0.38
Ce	58.1	47.9	82.0	0.19	0.51	3	0.01	0.47	0.41
Eu	1.02	0.90	0.95	1.27	0.68	1.5	0.02	0.89	1.12
Yb	1.37	1.35	1.60	0.3	1.3	1.8	0.07	1.51	0.74
Ni	69	17.6	17.6	0	5.9	29	36.4	5	3.34
Cr	289	52.4	3.93	0.02	9.7	153	0.7	0.95	8.35

	JL-AZU-004	wt.% 33.1		Mineral Kd's					
Sample	POR 10 01	JL-AZU-004	Cl Calculated	Plagioclase	Clinopyroxene	Magnetite	Olivine	Orthopyroxene	Bulk D
U	3.72	10.2	11.1	0.01	0.04	0	0.00	0	0.01
Ba	601	640	650	1.45	0.15	0.03	0.01	0.11	0.93
Nb	13.0	14.8	35.1	0.05	0.01	0.7	0.01	0.27	0.10
Zr	137	161	316	0.05	1.11	0.71	0.14	0.18	0.24
Y	16.9	19.1	33.7	0.2	1	0.2	0.01	0.54	0.38
Sr	560	281	312	2.41	0.12	0	0.01	0.21	1.53
Rb	46	215	138	0.01	0.00	0	0.00	0.01	0.01
La	37.1	35.8	77.5	0.28	0.19	3	0.01	0.26	0.33
Ce	58.1	69.8	117	0.19	0.51	3	0.01	0.47	0.37
Eu	1.02	0.85	0.92	1.27	0.68	1.5	0.02	0.89	1.09
Yb	1.37	2.18	1.88	0.3	1.3	1.8	0.07	1.51	0.72
Ni	69	13.9	14.4	0	4	29	2.2	5	2.42
Cr	289	14.5	1.24	0.02	10	153	0.7	0.95	5.94

	JL-AZU-006	wt. % 55.5		Mineral Kd's					
Sample	POR 10 01	JL-AZU-006	Cl Calculated	Plagioclase	Clinopyroxene	Magnetite	Olivine	Orthopyroxene	Bulk D
U	3.72	3.56	6.64	0.01	0.04	0	0.00	0	0.02
Ba	601	661	661	1.39	0.00	0	0.01	0.01	0.84
Nb	13.0	8.51	22.6	0.045	0.01	0.7	0.01	0.27	0.06
Zr	137	104	201	0.05	1.11	0.71	0.14	0.18	0.35
Y	16.9	13.1	24.4	0.2	1	0.2	0.01	0.54	0.38
Sr	560	502	502	1.94	0.06	0	0.01	0.04	1.18
Rb	46	91.8	82.6	0.01	0.00	0	0.00	0.01	0.01
La	37.1	22.2	54.3	0.28	0.19	3	0.01	0.26	0.35
Ce	58.1	45.3	83.9	0.19	0.51	3	0.01	0.47	0.38
Eu	1.02	0.88	1.02	1.27	0.68	1.5	0.02	0.89	1.00
Yb	1.37	1.38	1.74	0.3	1.3	1.8	0.07	1.51	0.59
Ni	69	21.5	21.5	0	5.8	29	2.2	5	2.98
Cr	289	55	2.05	0	9.7	153	0.7	0.95	9.40

	JL-AZU-008	wt. % 58.2		Mineral Kd's					
Sample	POR 10 01	JL - AZU - 008	Cl Calculated	Plagioclase	Clinopyroxene	Magnetite	Olivine	Orthopyroxene	Bulk D
U	3.72	3.57	7.13	0.01	0.04	0	0.00	0	0.02
Ba	601	688	707	1.42	0.03	0	0.01	0.01	0.75
Nb	13.0	9.36	24.3	0.05	0.01	10	0.01	0.27	0.07
Zr	137	116	199	0.05	1.11	0.71	0.14	0.18	0.47
Y	16.9	13.7	23.3	0.3	1	0.2	0.01	0.54	0.59
Sr	560	516	505	2.16	0.06	0	0.01	0.04	1.15
Rb	46	94.9	89.1	0.01	0.00	0	0.00	0.01	0.01
La	37.1	24.2	62.0	0.28	0.19	3	0.01	0.26	0.25
Ce	58.1	50.1	89.4	0.3	0.51	3	0.01	0.47	0.40
Eu	1.02	0.98	1.08	1.27	0.68	1.5	0.02	0.89	1.01
Yb	1.37	1.39	1.74	0.3	1.3	1.8	0.07	1.51	0.80
Ni	69	17.9	1.26	0	7.69	29	36.4	5	3.49
Cr	289	52.2	31.8	0.02	10.3	153	0.7	0.95	4.35

The modelled trace element data does not provide any definite conclusions regarding the evolution of the Azufre lavas. Within the model it is possible to approach the observed trace element results by adjusting partition coefficients, within a range that is accepted for the relevant partition coefficients. Assimilation of crustal material by the upwelling magma provides a potential explanation for the disconnect between what has been observed and what has been modelled. Assimilation can be seen as a plausible additional process to fractional crystallisation, based on other work that has been performed in the APVC that demonstrates AFC processes taking place in other volcanic centres in the APVC (Godoy et al., 2014, 2017; Michelfelder et al., 2014). Whereas the modelled trace element data is able to match the observed trace element data, for certain elements (Ba, Sr, and Ni), there are other elements where the model is unable to replicate the observed data. This is attributed to the sample POR 10 01 being used as a proxy parental magma and, while not necessarily representative of the ideal parental magma, is the closest to a a parental magma that is available.

To further identify how the Azufre lavas have evolved, radiogenic and stable isotope data are examined to provide insight into what role assimilation has played in the evolution process of the Azufre lavas, as fractionation alone does not account for isotopic variations.

7.3 Assimilation Processes

7.3.1 Radiogenic Isotopes

There are multiple correlations previously identified between the radiogenic isotope compositions of different volcanic centres of the APVC (Godoy et al., 2014, 2017; Michelfelder et al., 2014). There is a negative linear correlation between Sr and Nd (Fig. 10), and a more obvious correlation between $^{87}Sr/^{86}Sr$ and SiO_2 (Fig. 11) than there is between $^{143}Nd/^{144}Nd$ and SiO_2 (Fig. 12).

While Azufre‘s setting places it within the bounds of the APMB, it is also relatively close to the margins of it. This means that although Azufre has high Sr isotope ratios (relative to other Central Andean lavas) it, and in comparison the nearby volcanoes of the San Pedro-Linzor chain, has low Sr ratios compared to volcanoes which are situated near to the centre of the APMB ($\sim$0.707 vs. 0.710 0.717) (Godoy et al., 2017). When comparing the radiogenic isotope vs. SiO_2 plots of Azufre and the volcanoes of the SPLVC there are trends that become apparent. The data for $^{87}Sr/^{86}Sr$ ratios show a general trend of increasing Sr ratios with increasing SiO_2 to the south east, however the data from the two most south easterly volcanoes (Cerro del Leon and Toconce) overlaps to a large degree. The $^{143}Nd/^{144}Nd$ ratio data provide a more obvious trend where the Nd ratios decrease with increasing SiO_2 to the south east. These trends to the south east coincide with progression from the edge of the APMB towards the centre of the APMB, with the highest Sr ratios and the lowest Nd ratios being closest to the centre. There is a correlation between the $^{143}Nd/^{144}Nd$ and $^{87}Sr/^{86}Sr$ for Azufre and the SPLVC, where $^{87}Sr/^{86}Sr$ increases as $^{143}Nd/^{144}Nd$ decreases towards the south east, and the centre of the APMB.

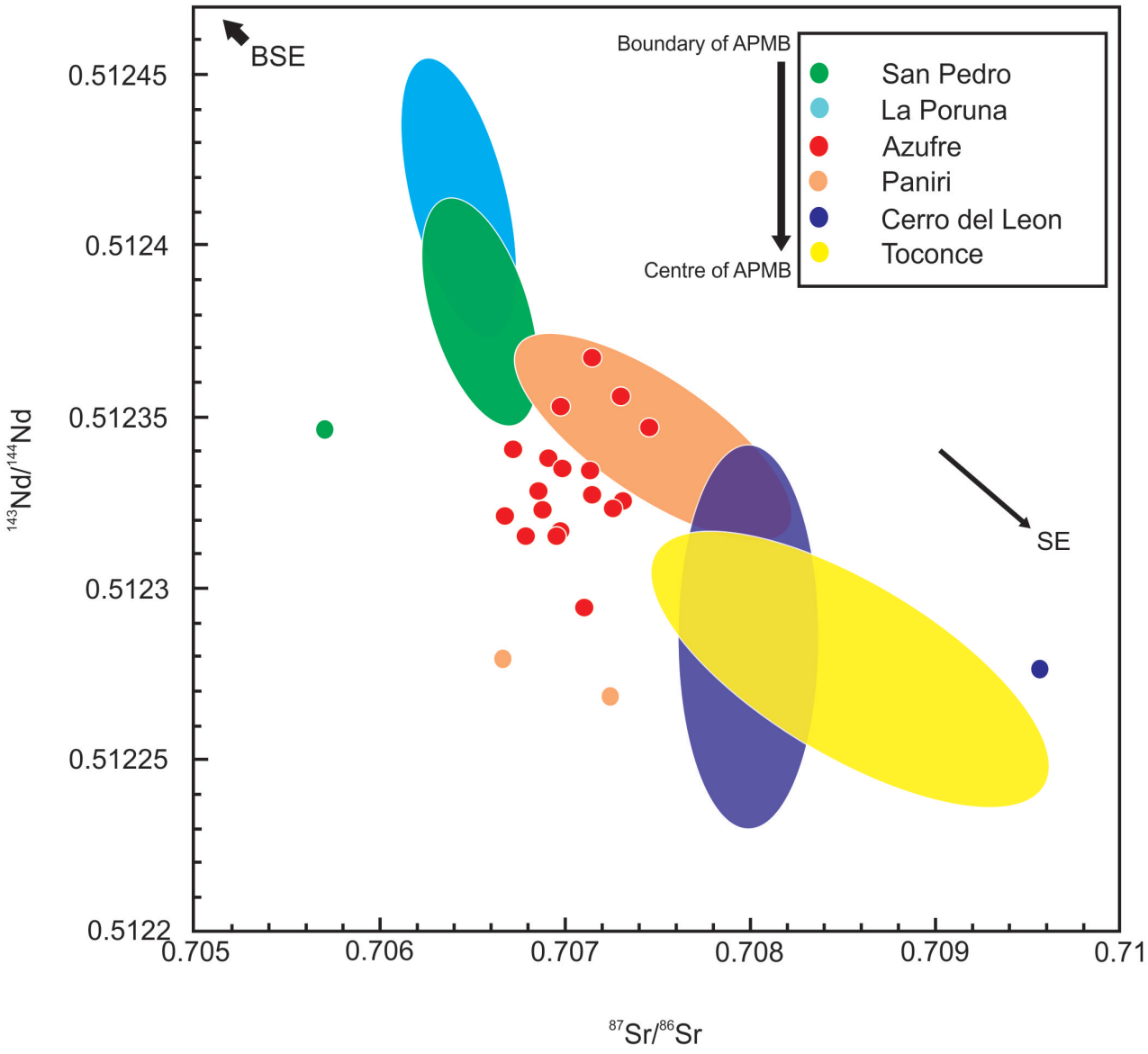

Figure 10: $^{143}Nd/^{144}Nd$ vs $^{87}Sr/^{86}Sr$ plot for analysed samples from Azufre and the SPLVC. SPLVC data from Godoy et al. (2017). Bulk Silicate Earth (BSE) $^{87}Sr/^{86}Sr$ and $^{143}Nd/^{144}Nd$ of 0.7045 and 0.512638, respectively, from Workman & Hart (2005)

The $^{87}Sr/^{86}Sr$ ratios for both Azufre and the volcanoes of the San Pedro - Linzor chain are significantly higher than the primitive mantle value and generally higher than the Sr "baseline" value of the CVZ (ca. 0.703 and 0.705 respectively) (Davidson et al., 1990; Godoy et al., 2014; Kay et al., 1994). That erupted lavas at Azufre are enriched in Sr relative to mantle values can be explained by contamination processes that were enacted on ascending primitive magmas, as they traverse through the thick continental crust of the CVZ. What remains to be examined is the degree to which this contamination occurs and the mechanism for it.

Sr-isotope data from Azufre were plotted together with San Pedro – Linzor chain data from Godoy et al. (2017) on a plot of Sr (ppm) vs. $^{87}Sr/^{86}Sr$, for comparison. The AFC model used in Godoy et al. (2017) was assessed to be relevant for use in this study, due to the proximity of Azufre to San Pedro. Data from Azufre fall into trends displayed by the volcanic centres of the SPLVC. Azufre displays values for major and trace element, and isotopic data (Fig. 13) that are correspondent with that of volcanoes of the SPLVC, especially of those volcanoes which it is situated near to (San Pedro and Paniri).

For the AFC model produced by Godoy et al. (2017) an uncontaminated end-member composition was taken from Matthews et al. (1994) for Lascar volcano. (Godoy et al., 2017) selected this sample due to its low $^{87}Sr/^{86}Sr$ ratio, which corresponds to isotopic baseline values established by Davidson et al. (1990); Blum-Oeste & Wörner (2016), SiO_2, and Mg number. The sample used to represent the Paleozoic Andean basement contaminant is a bulk felsic upper crustal composition from Sierra de Moreno. The crustal rocks from this region exhibit ranges in $^{87}Sr/^{86}Sr$ ratios (0.707 to 0.728), SiO_2 (54 to 69 wt.%), and Mg number (35 to 60). In order to model AFC processes the average Sr composition of this Paleozoic crust was used (Godoy et al., 2017; Lucassen et al., 2001). The data collected from Azufre are plotted in Fig. 13, with the data presented by Godoy et al. (2017). The model produced indicates that the proportion of assimilated crustal material, for Azufre lavas, is between 10 and 20 %, if the same end-members are assumed. The modelled assimilation for Azufre is approximately between that of San Pedro and Paniri, and helps to further define a trend of increasing assimilation from NW to SE.

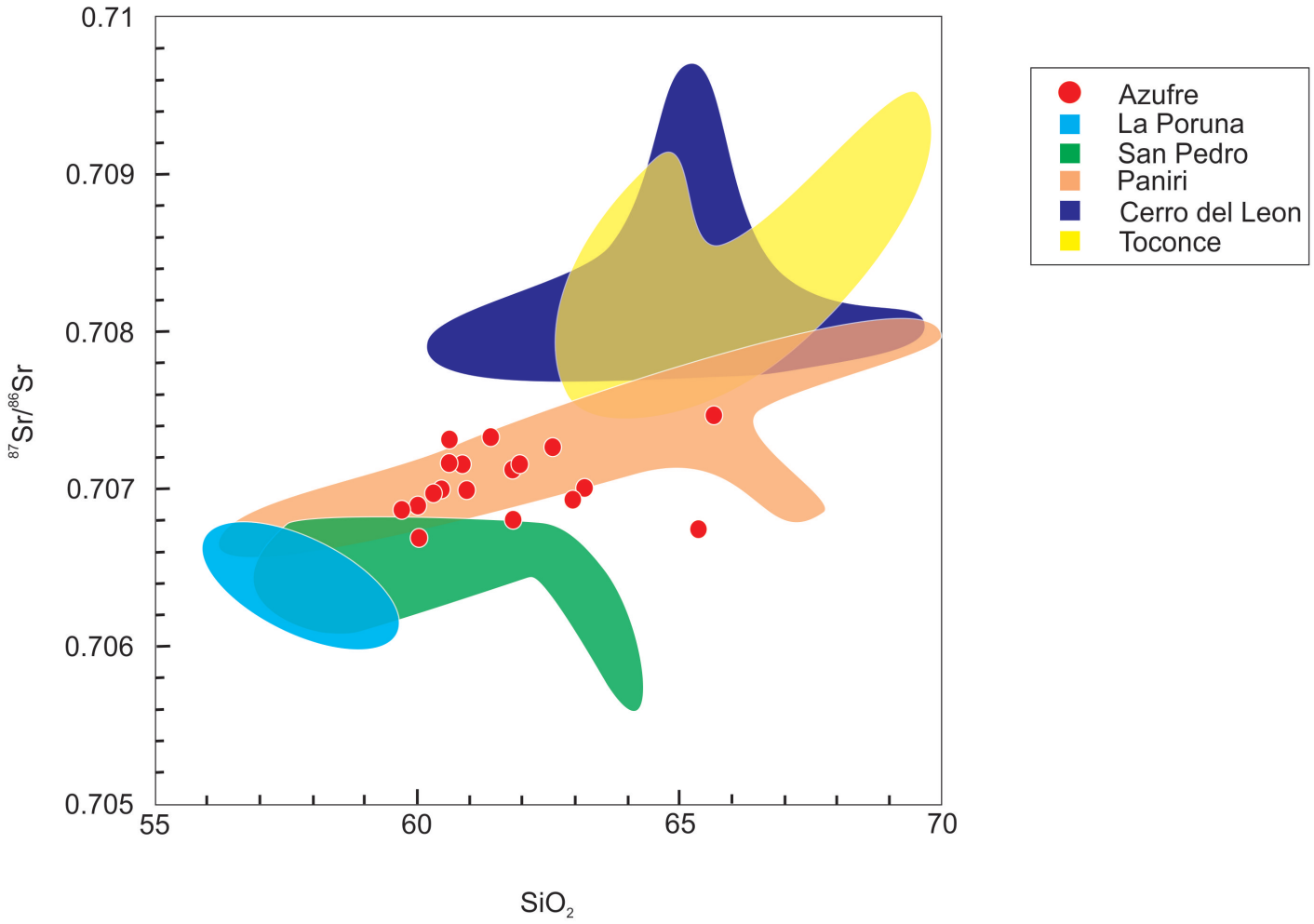

Figure 11: $^{87}Sr/^{86}Sr$ vs SiO_2 plot for analysed samples from Azufre and the SPLVC.

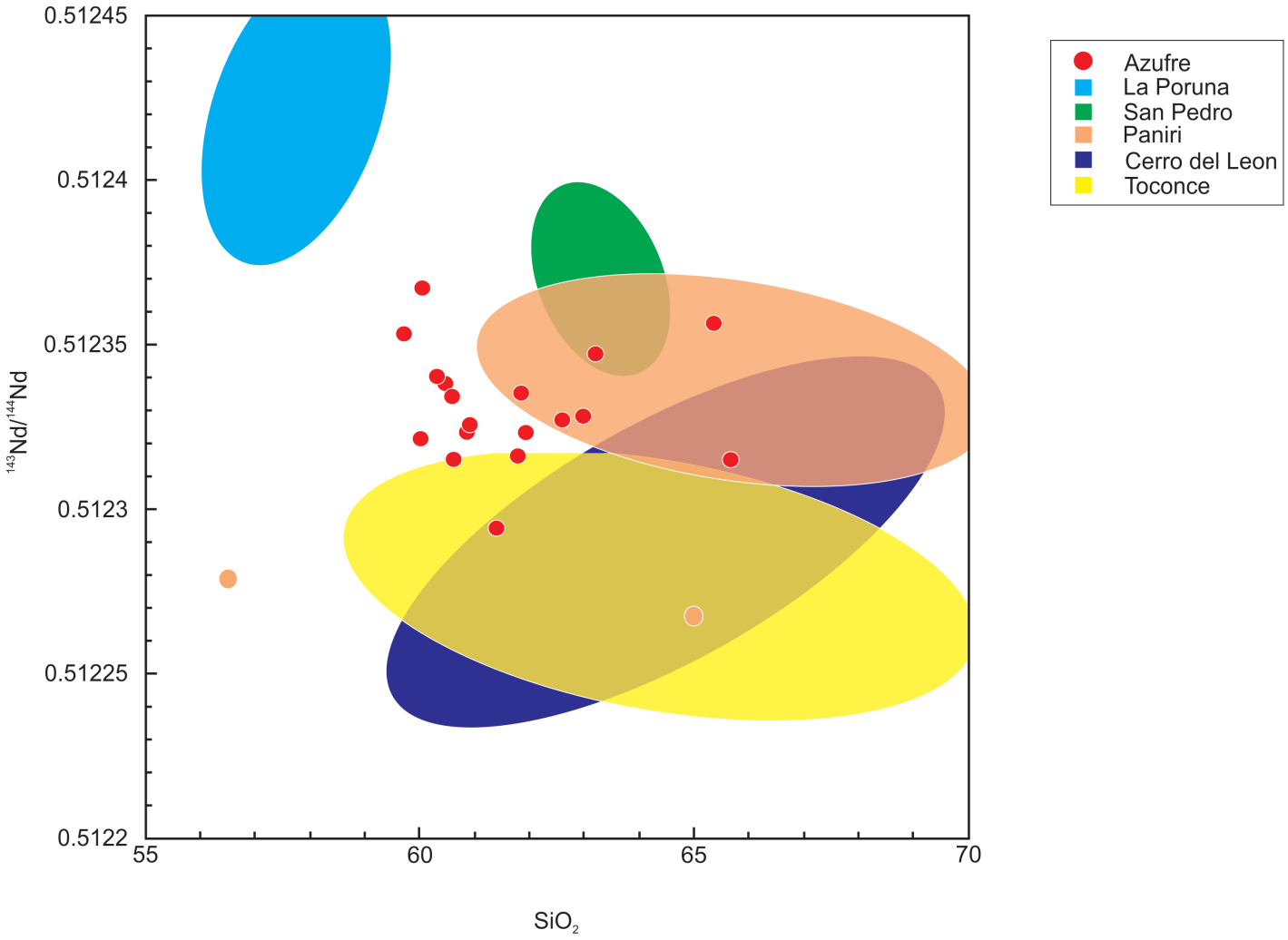

Figure 12: $^{143}Nd/^{144}Nd$ vs SiO_2 plot for analysed samples from Azufre and the SPLVC.

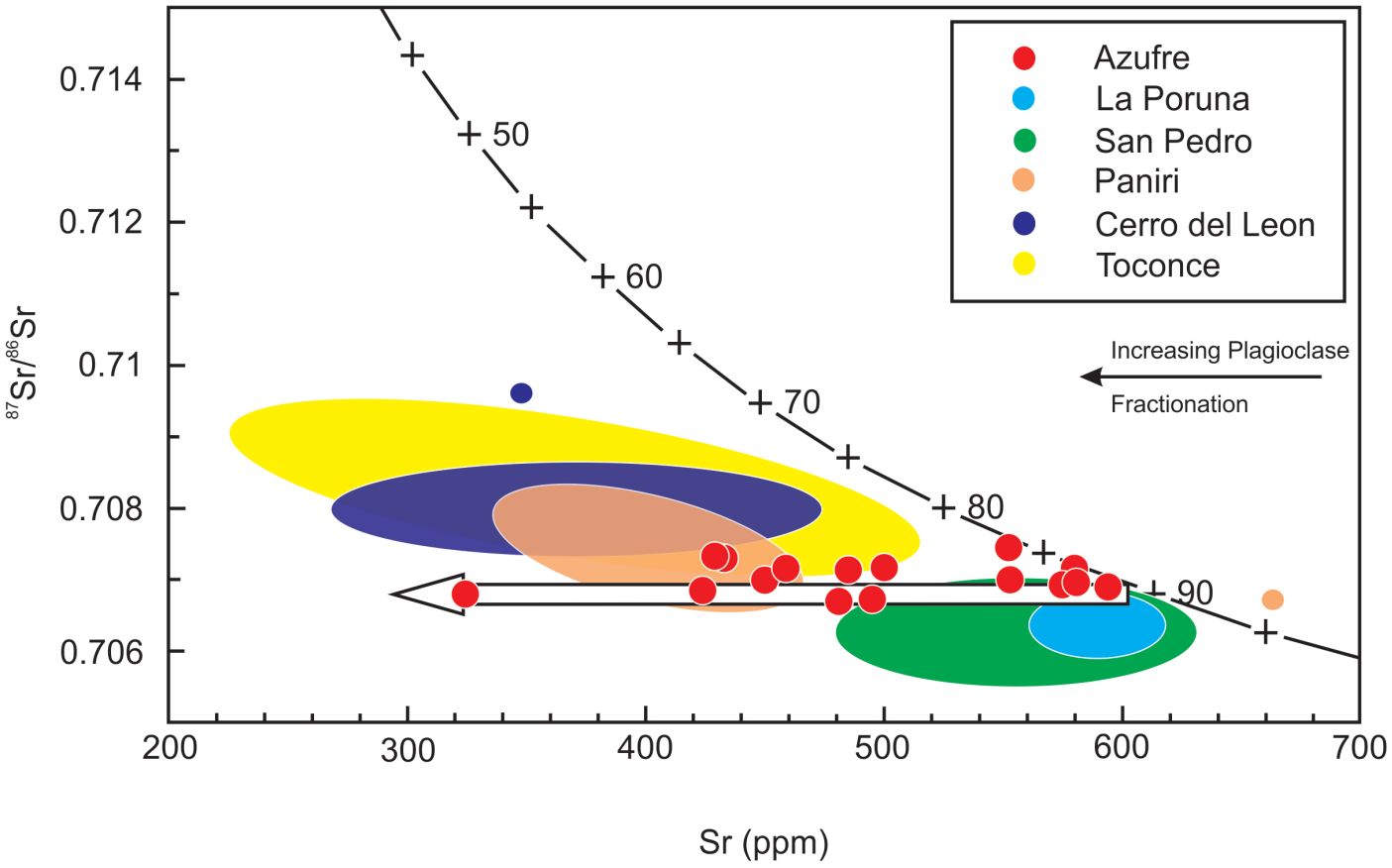

Figure 13: $^{87}Sr/^{86}Sr$ vs Sr (ppm)plot for analysed samples from Azufre and the SPLVC. The curve represents the AFC model produced by Godoy et al. (2017). The white arrow represents a proposed trend for closed system fractional crystallization starting from a magma that was initially formed by an AFC process. Numbers in italics indicate the estimated melt fraction remaining.

7.3.2 Stable Isotopes

The δ ^{18}O quartz values for Azufre lavas are all >7 ‰, which places them outside of the average mantle values of 5.5 to 5.9 ‰(Eiler, 2001; Iovine et al., 2016). Average sample δ ^{18}O range for Azufre is from 7.89 ‰to 11.95 ‰, however this maximum value is greater than the next highest, and stands out as an outlier, as the next highest value for any volcano of the APVC does not exceed 10 ‰. When it is treated as such the average range is between 7.89 ‰ and 9.55 ‰. By comparison, the volcanoes of Aucanquilcha (just outside the bounds of the APMB), Ollagüe (just inside the bounds of the APMB), and Uturuncu (at the centre of the APMB) have δ ^{18}O quartz ranges of 7 ‰- 7.3 ‰, 7.3 ‰- 8.3 ‰, and 7.3 ‰- 9.6 ‰, respectively (Michelfelder et al., 2013). These data indicate an increase in the range of δ ^{18}O from the edges of the APMB towards the centre, suggesting that the lavas erupted at the centre have had more interaction with the crust as they have traversed it.

When the data is examined without the outlying data point (Fig. 14) two arrays become evident. One array shows increasing δ ^{18}O quartz values with increasing ^{87}Sr/^{86}Sr, and decreasing δ ^{18}O quartz values with increasing ε_{Nd}, (A1) while the other shows decreasing δ ^{18}O with increasing ^{87}Sr/^{86}Sr, and increasing δ ^{18}O with increasing ε_{Nd} (A2). These two arrays indicate that there are likely to have been two separate sources of O enrichment. A1 is interpreted as representing the lavas which have undergone hydrothermal alteration, as well as assimilation of high δ ^{18}O crustal material, while A2 is interpreted as representing those lavas which have interacted with the crust purely through assimilation of low δ ^{18}O crustal material. A2 is unexpected for lavas that have undergone assimilation as normally δ ^{18}O would increase with interaction with the crust, due to it being expected that the crust would have high Sr and low Nd isotope ratios, and high δ ^{18}O rather than low δ ^{18}O. This discrepancy can be resolved by a localised area of the crust, in this region, displaying a low overall δ ^{18}O.

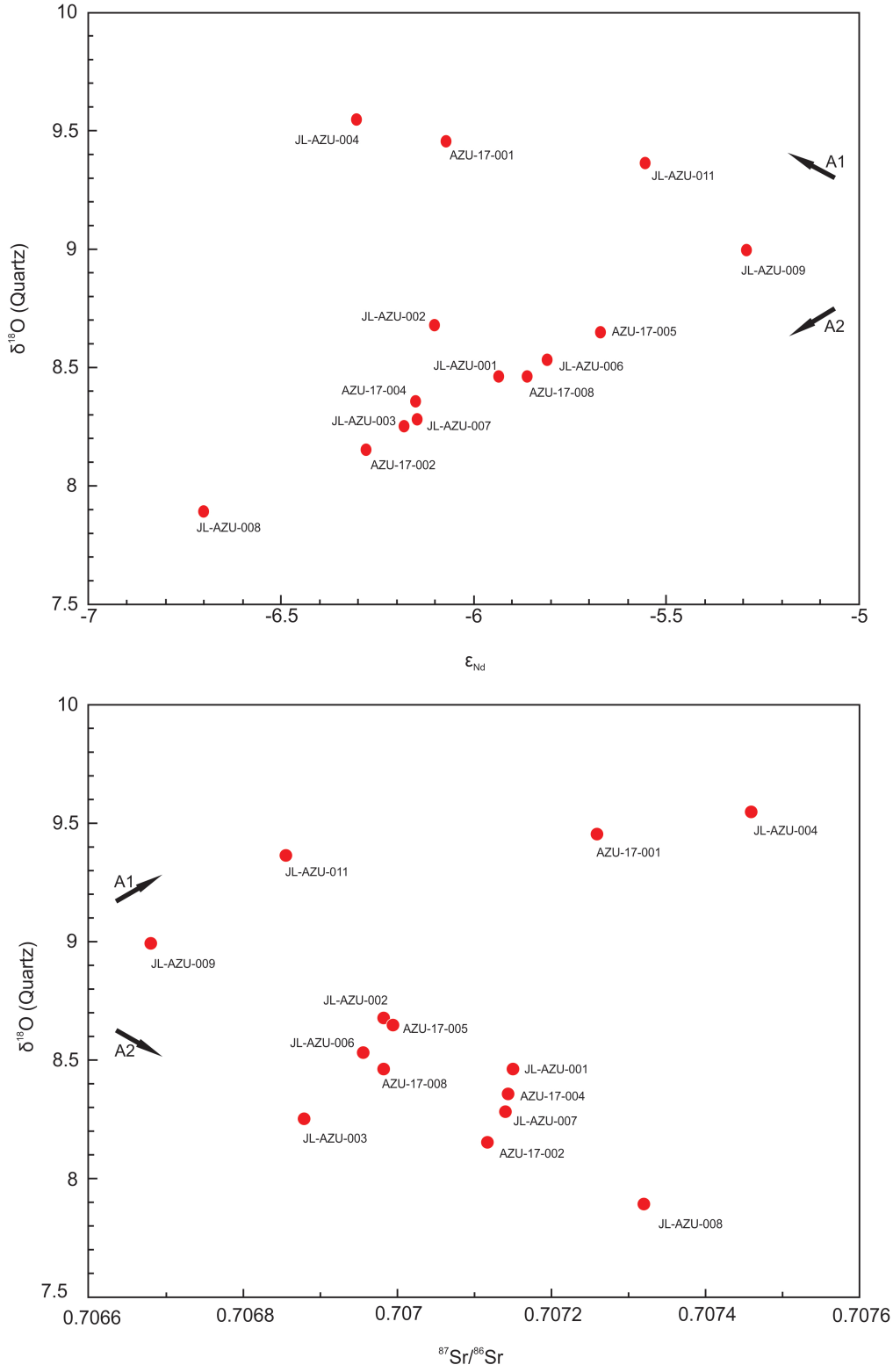

Figure 14: Plots of $\delta\ ^{18}O$ vs. ϵ_{Nd} and $\delta\ ^{18}O$ vs. $^{87}Sr/^{86}Sr$

Table 9: δ ^{18}O Model for lavas of Array A2 (Fig. 14)

$$\frac{\delta^{18}Ofinal - \delta^{18}Oinitial(1-x)}{x} = \delta^{18}Oassimilant$$

Where X is Mass Fraction[3]

	$_X$assimilant	δ ^{18}O assimilant (‰)
δ ^{18}O initial (8.99)		
	0.02	-46.01
	0.04	-18.51
	0.06	-9.34
	0.08	-4.76
	0.1	-2.01
	0.12	-0.18
	0.14	1.13
	0.16	2.12
	0.18	2.88
	0.2	3.49
	0.5	6.79
δ ^{18}O final (7.89)	1	7.89

[3]Mass balance calculation modelling δ ^{18}O for given Mass Fractions of assimilating material, where $_x$assimilant for Azufre is between 0.1 and 0.2 (Fig. 13).

The δ ^{18}O of the upper crustal contaminant can be modelled, using mass balance equations, to determine whether the contaminant is either depleted or enriched in δ ^{18}O. The results of these calculations are displayed in Table 9. These results show that for the 10 - 20% assimilation indicated by the AFC model in Figure 12 the upper crustal contaminant would require a δ ^{18}O between -2.01 and 3.49 ‰. This suggests that there is a region located below Azufre, at shallow crustal depths, that is depleted in ^{18}O.

Feeley & Sharp (1995) studied the δ ^{18}O of Ollagüe, and proposed a two stage process of magmatic evolution where first a basaltic parent facilitates melting in a high δ ^{18}O lower crust (assimilation) followed by fractional crystalisation of the resultant intermediate magmas at shallow crustal depths. This model does not make allowance for the APMB, the presence of which could have an effect on the depths of the different stages of evolution. The existence of the APMB could mean that the interactions between crust and parent magmas occur far shallower than Feeley & Sharp (1995) describe, such as multiple stages of assimilation in the lower, middle, and upper crust. The lack of a garnet crystallisation signature in the Azufre, and SPLVC, data supports the idea that AFC processes are occurring at shallow crustal depths, within the geographical limits of the APMB at least and not necessarily in the rest of the Andes.

The two arrays displayed in Fig. 14 are not completely comparable to those of Feeley & Sharp (1995) which describe a process where magmatic evolution of Ollagüe is a single, two-stage process of an initial, deep AFC process followed by a shallow AFC process, with lower r. This proposed model does not explain the combined oxygen, trace element, and radiogenic isotope compositional variation which are observed for Azufre. By superimposing a map of Azufre (Hübner Gonzalez, 2018) over the Google Earth image showing this study's sample locations it is possible to identify the different lava flows which the samples were collected from, and therefore also provide ages for the different samples (Fig. 15). The inconsistency between this study and Feeley & Sharp (1995) is addressed by A1 and A2 being representative of differently aged lava flows. A1 contains samples from Unit 2 while A2 contains samples from Units 1 and 4. There are 3 samples from Unit 3 that are represented on Fig. 14, however one of these samples is in A1, one is in A2, and the third sample is the irregularly high δ ^{18}O sample, making it impossible to determine how Unit 3 fits into the magmatic history of Azufre, without further samples. Based on the research of Hübner Gonzalez (2018) the three, relevant magmatic events can be ordered with Unit 1 occurring 1500 ka, Unit 2 600 ka, and Unit 4 100-150 ka. By now looking at the two arrays as separate events, as opposed to two stages of a single event, it is possible to reconcile the δ ^{18}O data with the elemental and radiogenic isotopic data to explain the magmatic history of Azufre.

In order to produce the two arrays seen in Fig. 14 the eruptive events that resulted in the different lava flows must have experienced different magmatic processes to each other. A1 represents a magmatic event that would have assimilated high δ ^{18}O crustal material, whereas A2 shows two magmatic events that would have each assimilated low δ ^{18}O crustal material. In addition to the arrays being representative of different flows A2 itself consists of two separate flows. The two flows of A2 are significantly different ages to each other, and to that of A1. The flows in A2 are 150ka and 1500ka respectively, whereas the flow in A1 is 600ka. A fourth flow is represented

in the data, however there are not enough samples from it to be able to constrain it with regards to the other flows.

This presents a scenario where there has been an eruption where low δ ^{18}O crustal material has been assimilated, followed by an eruption where high δ ^{18}O crustal material has been assimilated, and then this has subsequently been followed by a third eruption where once again low δ ^{18}O crustal material has been assimilated. The research performed by Hübner Gonzalez (2018) provides a means of explaining this by having identified multiple conduits via which the different flows have been transported (Fig. 16). The number of different conduits could be due to the presence of a lineament striking directly through Azufre (Tibaldi et al., 2009). For A2 the δ ^{18}O value decreases as the chemical evolution of Azufre increases, indicating that the crustal material that was assimilated has been altered hydrothermally. This alteration is most likely due to high-temperature interaction with meteoric water, the circulation of which was likely facilitated by the aforementioned lineaments (Feeley & Sharp, 1995; Rose et al., 1994).

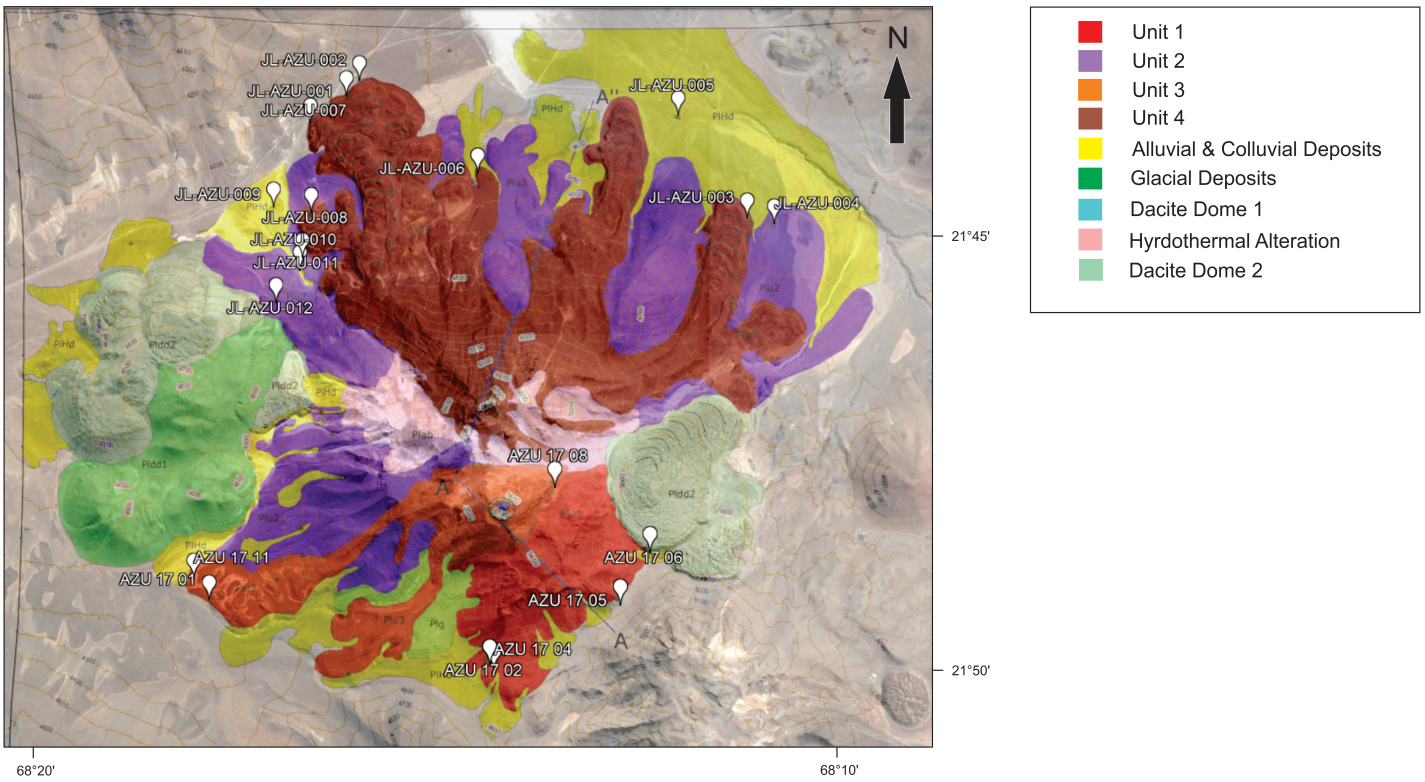

Figure 15: Superimposition of (Hübner Gonzalez, 2018) Azufre map over a satellite image of Azufre.
21°52'41.55"S and 68°20'17.23"W. **Google Earth**. May 05, 2016. November 07, 2016.

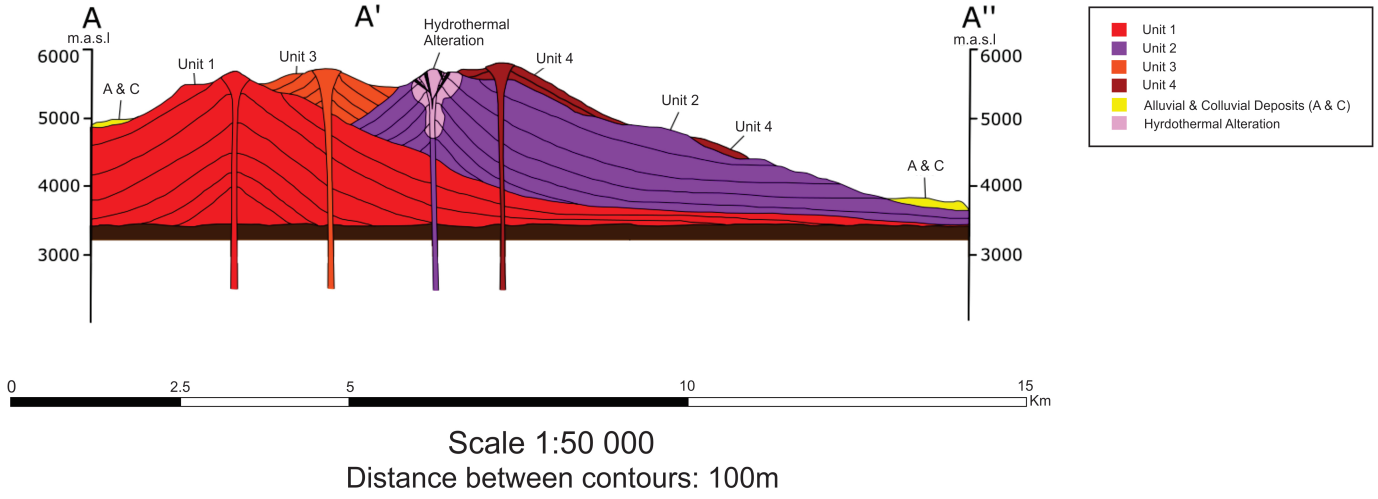

Figure 16: Cross Section of Azufre, after (Hübner Gonzalez, 2018)

7.4 Summary

Major element modelling of Azufre lava samples gives between 42% and 67% fractional crystallisation with assemblages of: 22% - 41% plagiocase, 5.83% - 16.1% clinopyroxene, 0% - 13.1% orthopyroxene, 0.011% - 4.76% olivine, and 0.078% - 2.02% Fe-Ti oxides. Trace element modelling of Azufre lava samples does not provide any conclusive evidence regarding the evolution of Azufre due to discrepancies between the calculated and observed trace element values, however these discrepancies are partially explained by the fact that the sample used to represent the parental magma (POR 10 01) is merely representative as there are no samples, or available data, of actual parental magmas in the APVC. Isotopic data, both radiogenic and stable, suggest assimilation as a process that is occurring, along with fractional crystallisation. Radiogenic isotope data suggests that the amount of assimilation experienced by rising magmas was between 10% and 20%. Comparison of radiogenic isotopes from Azufre and volcanoes of the SPLVC indicate that the amount of assimilation undergone at different volcanic centres increases towards the south east, and the centre of the APMB. Stable isotope data shows that there must have been two separate sources of O enrichment, as there are 2 separate $\delta\ ^{18}O$ arrays that cannot be explained as two steps of the same process. These two arrays suggest that magma has, during different events, assimilated either high or low $\delta\ ^{18}O$ crustal material, a process which therefore require multiple conduits to the surface and magma chambers situated at different depths so as to account for why this interaction has differed between eruptive events.

8 Conclusion

Lavas erupted at Azufre represent geochemical and isotopic characteristics that are particular to the Altiplano-Puna Volcanic Complex (APVC) and which differ from conventional recent Central Andean volcanoes.

- REE patterns from Azufre display low LREE/HREE ratios and do not show the high-P garnet crystallisation signature which is characteristic of Central Andean lavas, despite traversal through the region's exceptionally thick crust (up to 70 km). Azufre also displays a negative Eu anomaly that is significantly stronger than that seen in conventional Central Andean lavas. These factors suggest extensive plagioclase fractionation at shallow crustal depths.
- Fractional crystallisation was modelled for 4 samples ,with fractional crystallisation amounts of 44%, 67%, 45%, and 48% (JL-AZU-001, -004, -006, and -008 respectively). Mineral assemblages:
  - JL-AZU-001: Plagioclase : Clinopyroxene : Orthopyroxene : Olivine : Fe-Oxide = 61.56 : 13.29 : 19.9 : 0.75 : 4.54
  - JL-AZU-004: Plagioclase : Clinopyroxene : Orthopyroxene : Olivine : Fe-Oxide = 61.17 : 14.08 : 19.54 : 2.39 : 2.82
  - JL-AZU-006: Plagioclase : Clinopyroxene : Orthopyroxene : Olivine : Fe-Oxide = 60.29 : 24.56 : 0 : 10.63 : 4.51
  - JL-AZU-008: Plagioclase : Clinopyroxene : Orthopyroxene : Olivine : Fe-Oxide = 52.32 : 38.29 : 9.18 : 0.026 : 0.185
- Azufre shows high $^{87}Sr/^{86}Sr$ isotopic ratios, which have been related to AFC-type contamination of upwelling magmas by between 10% and 20% upper crustal material.
- From this data, and Azufre's location on the margins of the Altiplano-Puna Magma Body (APMB), it is interpreted that Azufre lavas evolved in S-MASH (shallow melting, assimilation, storage, homogenisation) zones, rather than the MASH (melting, assimilation, storage, homogenisation) zones conventionally proposed for Central Andean magmatic evolution.
- Stable isotope data from Azufre reveals that there were multiple magmatic series produced pre-eruption, with assimilation of either high or low $\delta\ ^{18}O$ crustal material. Assimilation of high $\delta\ ^{18}O$ material is interpreted to be associated with the APMB while low $\delta\ ^{18}O$ is interpreted to be related to hydrothermal alteration due to the influence of meteoric water.
- Comparison of data from Azufre and other volcanoes of the APVC (San Pedro — Linzor Chain, Aucanquilcha, Ollagüe, and Uturuncu) reveals trends in elemental and isotopic data.
  - Major element data identify the lavas of the APVC as members of the high-K, calc-alkaline major oxide series, while trace element data indicate that magmatic evolution of volcanoes in the APVC did not occur at depth, expressed by flatter REE patterns than in conventional Central Andean volcanic centres and negative Eu anomalies.

  - Radiogenic isotope data displays overall trends of increasing $^{87}Sr/^{86}Sr$ and $\delta\ ^{18}O$, and decreasing $^{143}Nd/^{144}Nd$ towards the centre of the APVC.
  - These trends correlate with the increasing thickness of the APMB, with the lowest $^{87}Sr/^{86}Sr$ and $\delta\ ^{18}O$, and the highest $^{143}Nd/^{144}Nd$ relating to peripheries of the APMB and the opposite for the centre.
  - $^{87}Sr/^{86}Sr$ values also indicate a trend in increasing assimilation towards the centre of the APMB.

- The data collected from Azufre further asserts the fundamental role which the APMB has in the evolution of magmas within the APVC, however it also identifies that this evolution does not necessarily end with interaction between the APMB and upwelling magmas. Interaction between upwelling magmas and localised areas of low $\delta\ ^{18}O$ can lead to further evolution of magmas, post interaction with the APMB.

9 Acknowledgements

This dissertation would not have been possible without the encouragement, input, and support of a number of people, who have been with me for the ups and the downs of my MSc.

A very special thanks must go to Dr. Petrus le Roux for his role as my principal supervisor. Without his advice, guidance, and support this project would not have been possible and I am eternally grateful for his continual input and engagement throughout the process of it.

Special thanks must also go to Prof. Chris Harris for his role as my secondary supervisor, and for his advice and expertise that he lent to this project.

Many parts of this project would not have been possible without the help of the technical staff at the UCT Geology Department who helped me with the preparation and analysis of samples, their assistance was invaluable.

To our collaborators in Chile, muchas gracias por todo. Thank you Andrew for hosting me in Antofagasta (and for your help in getting through customs with crushed rock samples that looked slightly suspect in airport security x-rays). Thank you to Benigno and Osvaldo for taking me to La Poruna resort, helping with sample collection, and the input you've provided to the project.

And finally to my friends and family who have provided me with the emotional and financial support that has made this possible, your love and kindness has been incredible and I am so grateful to all of you.

I will lift up mine eyes unto the hills, from whence cometh my help. My help cometh from the Lord, which made heaven and earth.

References

Aitcheson, S. J. (1995). Pb isotopes define basement domains of the Altiplano, central Andes. *Geology*, 23(6), 555–558.

Allmendinger, R. W., Jordan, T. E., Kay, S. M., & Isacks, B. L. (1997). The evolution of the Altiplano-Puna Plateau of the central Andes. *Annual Review of Earth and Planetary Sciences*, 25(1), 139–174.

Baby, P., Rochat, P., Mascle, G., & Herail, G. (1990). Neogene shortening contribution to crustal thickening in the back arc of the central Andes. *Geology*, 25(10), 883–886.

Baumont, D., Paul, A., Zandt, G., Beck, S. L., & Pedersen, H. (2002). Lithospheric structure of the Central Andes based on surface wave dispersion. *Journal of Geophysical Research*, 107(B12), 18.1–18.13.

Beck, S. L., Zandt, G., Myers, S. C., Wallace, T. C., Silver, P. G., & Drake, L. (1996). Crustal-thickness variations in the central Andes. *Geology*, 24(5), 407–410.

Blum-Oeste, M. & Wörner, G. (2016). Central Andean magmatism can be constrained by three ubiquitous end-members. *Terra Nova*, 28(6), 434–440.

Chernicoff, C. J., Richards, J. P., & Zappettini, E. O. (2002). Crustal lineament control on magmatism and mineralization in northwestern Argentina: Geological, geophysical, and remote sensing evidence. *Ore Geology Reviews*, 21(3-4), 127–155.

Chmielowski, J., Zandt, G., & Haberland, C. (1999). The central Andean AltiplanoPuna magma body. *Geophysical Research Letters*, 26(6), 783–786.

Davidson, J. P., McMillan, N. J., Moorbath, S., Wörner, G., Harmon, R. S., & Lopez-Escobar, L. (1990). The Nevados de Payachata volcanic region (18S/69W, N. Chile) II. Evidence for widespread crustal involvement in Andean magmatism. *Contributions to Mineralogy and Petrology*, 105(4), 412–432.

de Silva, S. L. (1989). Altiplano-Puna volcanic complex of the central Andes. *Geology*, 17(12), 1102–1106.

de Silva, S. L. & Gosnold, W. D. (2007). Episodic construction of batholiths: Insights from the spatiotemporal development of an ignimbrite flare-up. *Journal of Volcanology and Geothermal Research*, 167(1-4), 320–335.

de Silva, S. L. & Kay, S. M. (2018). Turning up the heat: High-flux magmatism in the central andes. *Elements*, 14(4), 245–250.

de Silva, S. L., Self, S., Francis, P., Drake, R., & Carlos, R. (1994). Effusive silicic volcanism in the central Andes: The Chao dacite and other young lavas of the Altiplano-Puna Volcanic Complex. *Journal of Geophysical Research*, 99(B9), 17805–17825.

de Silva, S. L., Zandt, G., Trumbull, R. B., Viramonte, J. G., Salas, G., & Jiménez, N. C. (2006). Large ignimbrite eruptions and volcano-tectonic depressions in the Central Andes: a thermomechanical perspective. *Geological Society, London, Special Publications*, 269(1), 47–63.

Dickinson, W. R. (1975). Potash-Depth (K-h) relations in continental margin and intra-oceanic magmatic arcs. *Geology*, 3(2), 53–56.

EarthRef.org (2018). *Geochemical Earth Reference Model*. [Database].

Eiler, J. M. (2001). Oxygen isotope variations of basaltic lavas and upper mantle rocks. *Reviews in Mineralogy and Geochemistry*, 43(1), 319–364.

Feeley, T. C. & Sharp, Z. D. (1995). 18O/16O isotope geochemistry of silicic lava flows erupted from Volcan Ollague, Andean Central Volcanic Zone. *Earth and Planetary Science Letters*, 133(3-4), 239–254.

Fowler, C. M. R. (2005). *The solid earth*. Cambridge. England: Cambridge University Press, 2 edition.

Freymuth, H., Brandmeier, M., & Wörner, G. (2015). The origin and crust/mantle mass balance of Central Andean ignimbrite magmatism constrained by oxygen and strontium isotopes and erupted volumes. *Contributions to Mineralogy and Petrology*, 169(6), 58[1–24].

Godoy, B., Wörner, G., Kojima, S., Aguilera, F., Simon, K., & Hartmann, G. (2014). Low-pressure evolution of arc magmas in thickened crust: The San Pedro-Linzor volcanic chain, Central Andes, Northern Chile. *Journal of South American Earth Sciences*, 52, 24–42.

Godoy, B., Wörner, G., Le Roux, P., de Silva, S. L., Parada, M. A., Kojima, S., Gonzalez-Maurel, O., Morata, D., Polanco, E., & Martínez, P. (2017). Sr- and Nd- isotope variations along the Pleistocene San Pedro-Linzor volcanic chain, N. Chile: Tracking the influence of the upper crustal Altiplano-Puna Magma Body. *Journal of Volcanology and Geothermal Research*, 341, 172–186.

Harris, C. & Vogeli, J. (2011). Oxygen isotope composition of garnet in the peninsula granite, Cape Granite Suite, South Africa: Constraints on melting and emplacement mechanisms. *South African Journal of Geology*, 114(3-4), 387–414.

Hübner Gonzalez, D. S. (2018). *Evolución geológica del Volcán Azufre, II Región de Antofagasta*. (PhD Thesis) Department of Geology, University of Chile.

Iovine, R. S., Mazzeo, F. C., Arienzo, I., D'Antonio, M., Wörner, G., Civetta, L., Pastore, Z., & Orsi, G. (2016). Source and magmatic evolution inferred from geochemical and Sr-O-isotope data on hybrid lavas of Arso, the last eruption at Ischia island (Italy; 1302AD). *Journal of Volcanology and Geothermal Research*, 331, 1–15.

Kay, S. M., Coira, B. L., Caffe, P. J., & Chen, C. H. (2010). Regional chemical diversity, crustal and mantle sources and evolution of central Andean Puna plateau ignimbrites. *Journal of Volcanology and Geothermal Research*, 198(1-2), 81–111.

Kay, S. M., Coira, B. L., & Viramonte, J. G. (1994). Young mafic back arc volcanic rocks as indicators of continental lithospheric delamination beneath the Argentine Puna Plateau, central Andes. *Journal of Geophysical Research*, 99(B12), 24323–24339.

Kay, S. M., Mpodozis, C., & Coira, B. L. (1996). *Central Andean mantle-derived basalts and neogene mantle enrichment beneath the Puna Plateau.* Paper presented at the Thrid International Symposium on Andean Geodynamics (ISAG), St Malo, France, 17-19 September.

Leidig, M. & Zandt, G. (2003). Modeling of highly anisotropic crust and application to the Altiplano-Puna volcanic complex of the central Andes. *Journal of Geophysical Research*, 108(B1), 1–15.

Lucassen, F., Becchio, R., Harmon, R. S., Kasemann, S., Franz, G., Trumbull, R. B., Wilke, H.-G., Romer, R. L., & Dulski, P. (2001). Composition and density model of the continental crust at an active continental margin: The central Andes between 21 and 27S. *Tectonophysics*, 341(1-4), 195–223.

Mamani, M., Tassara, A., & Wörner, G. (2008). Composition and structural control of crustal domains in the central Andes. *Geochemistry, Geophysics, Geosystems*, 9(3), 1–13.

Mamani, M., Wörner, G., & Sempere, T. (2010). Geochemical variations in igneous rocks of the Central Andean orocline (13S to 18S): Tracing crustal thickening and magma generation through time and space. *Bulletin of the Geological Society of America*, 122(1-2), 162–182.

Matthews, S. J., Jones, A. P., & Gardeweg, M. C. (1994). Lascar volcano, northern Chile: Evidence for steady-state disequilibrium. *Journal of Petrology*, 35(2), 401–432.

McQuarrie, N., Horton, B. K., Zandt, G., Beck, S. L., & DeCelles, P. G. (2005). Lithospheric evolution of the Andean fold-thrust belt, Bolivia, and the origin of the central Andean plateau. *Tectonophysics*, 399, 15–37.

Michelfelder, G. S., Feeley, T. C., & Wilder, A. D. (2014). The volcanic evolution of Cerro Uturuncu: A high-K, composite volcano in the back-arc of the central Andes of SW Bolivia. *International Journal of Geosciences*, 5(11), 1263–1281.

Michelfelder, G. S., Feeley, T. C., Wilder, A. D., & Klemetti, E. W. (2013). Modification of the continental crust by subduction zone magmatism and vice-versa: Across-strike geochemical variations of silicic lavas from individual eruptive centers in the Andean Central Volcanic Zone. *Geosciences*, 3(4), 633–667.

Míková, J. & Denková, P. (2007). Modified chromatographic separation scheme for Sr and Nd isotope analysis in geological silicate samples. *Journal of Geosciences*, 52(3-4), 221–226.

Pin, C. & Santos Zalduegui, J. F. (1997). Sequential separation of light rare-earth elements, thorium and uranium by miniaturized extraction chromatography: Application to isotopic analyses of silicate rocks. *Analytica Chimica Acta*, 339(1-2), 79–89.

Prezzi, C. B., Gotze, H. J., & Schmidt, S. (2009). 3D density model of the central Andes. *Physics of the Earth and Planetary Interiors*, 177(3-4), 217–234.

Rickwood, P. C. (1989). Boundary lines within petrologic diagrams which use oxides of major and minor elements. *Lithos*, 22(4), 247–263.

Riller, U., Petrinovic, I. A., Ramelow, J., Strecker, M., & Oncken, O. (2001). Late cenozoic tectonism, collapse caldera and plateau formation in the Central Andes. *Earth and Planetary Science Letters*, 188(3-4), 299–311.

Rose, T. P., Criss, R. E., Mughannam, A. J., & Clynne, M. A. (1994). Oxygen isotope evidence for hydrothermal alteration within a Quaternary stratovolcano, Lassen Volcanic National Park, California. *Journal of Geophysical Research*, 99633(10), 621–21.

Schmitt, A., de Silva, S. L., Trumbull, R. B., & Emmermann, R. (2001). Magma evolution in the Purico ignimbrite complex, northern Chile: evidence for zoning of a dacitic magma by injection of rhyolitic melts following mafic recharge. *Contributions to Mineralogy and Petrology*, 140(6), 680–700.

Schurr, B., Asch, G., Rietbrock, A., Trumbull, R. B., & Haberland, C. (2003). Complex patterns of fluid and melt transport in the central Andean subduction zone revealed by attenuation tomography. *Earth and Planetary Science Letters*, 215(1-2), 105–119.

Sun, S.-s. & McDonough, W. F. (1989). Chemical and isotopic systematics of oceanic basalts: implications for mantle composition and processes. *Geological Society, London, Special Publications*, 42(1), 313–345.

Taylor, S. R. & McLennan, S. M. (1988). The significance of the rare earths in geochemistry and cosmochemistry. In K. Gschneidner & L. Eyring (Eds.), *Handbook on the Physics and Chemistry of Rare Earths* (pp. 485–578). London, England: Elsevier.

Tibaldi, A., Corazzato, C., & Rovida, A. (2009). Miocene-Quaternary structural evolution of the Uyuni-Atacama region, Andes of Chile and Bolivia. *Tectonophysics*, 471(1-2), 114–135.

Trumbull, R. B., Ulrich, R., Oncken, O., Ekkehard, S., Munier, K., & Hongn, F. (2006). The time-space distribution of Cenozoic volcanism in the south-central Andes: A new data compilation and some tectonic implications. In O. Oncken, G. Chong, G. Franz, P. Giese, H.-J. Götze, V. A. Ramos, M. R. Strecker, & P. Wigge (Eds.), *The Andes: Active Subduction Orogeny* (pp. 29–43). Berlin, Germany: Elsevier.

Ward, K. M., Zandt, G., Beck, S. L., Christensen, D. H., & McFarlin, H. (2014). Seismic imaging of the magmatic underpinnings beneath the Altiplano-Puna volcanic complex from the joint inversion of surface wave dispersion and receiver functions. *Earth and Planetary Science Letters*, 404, 43–53.

Workman, R. K. & Hart, S. R. (2005). Major and trace element composition of the depleted MORB mantle (DMM). *Earth and Planetary Science Letters*, 231(1-2), 53–72.

Zandt, G., Leidig, M., Chmielowski, J., Baumont, D., & Yuan, X. (2003). Seismic detection and characterization of the Altiplano-Puna Magma Body, central Andes. *Pure and Applied Geophysics*, 160(3), 789–807.

10 Appendix

Table 10: Probe Data, Plagioclase

Sample	SiO_2	TiO_2	Al_2O_3	FeO	MnO	MgO	CaO	Na_2O	K_2O	Total
AZU-001_L1_G1_C1	58.14	0.006	26.833	0.261	0.026	0.011	8.354	6.392	0.54	100.563
AZU-001_L1_G1_C2	58.739	0.025	26.261	0.21	0	0	7.992	6.529	0.566	100.322
AZU-001_L1_G1_C3	58.227	0	26.778	0.212	0	0.007	8.433	6.462	0.505	100.624
AZU-001_L1_G1_C4	58.314	0.029	26.382	0.214	0	0	8.273	6.347	0.576	100.135
AZU-001_L1_G1_R1	54.764	0.069	28.903	0.441	0.014	0.045	11.372	4.945	0.307	100.86
AZU-001_L2_G2_C1	56.844	0.038	27.585	0.228	0.034	0.005	9.603	5.694	0.45	100.481
AZU-001_L2_G2_R1	59.984	0.029	25.526	0.208	0.014	0.007	7.301	6.926	0.69	100.685
AZU-001_L3_G3_C1	58.723	0.04	25.577	0.198	0.02	0.01	7.654	6.486	0.641	99.349
AZU-001_L3_G3_R1	58.932	0.031	25.637	0.254	0.019	0.013	7.871	6.724	0.608	100.089
AZU-001_L4_G4_C1	57.604	0.022	26.543	0.239	0.017	0.001	8.567	6.392	0.495	99.88
AZU-001_L4_G4_R1	58.368	0.024	26.322	0.365	0	0.024	8.322	6.288	0.43	100.143
AZU-002_L1_G1_C1	58.267	0	25.845	0.283	0	0.003	8.009	6.703	0.601	99.711
AZU-002_L1_G1_R1	58.826	0	25.496	0.27	0.005	0.041	7.554	6.931	0.679	99.802
AZU-002_L2_G2_C1	58.887	0.047	25.501	0.236	0	0.001	7.593	6.862	0.699	99.826
AZU-002_L2_G2_R1	58.798	0.002	25.378	0.217	0.023	0.026	7.451	6.766	0.694	99.355
AZU-002_L3_G3_R1	59.199	0.016	25.407	0.307	0.027	0.026	7.457	6.641	0.727	99.807
AZU-002_L4_G4_C1	56.714	0.029	26.526	0.235	0	0.01	8.882	6.133	0.513	99.042
AZU-002_L4_G4_R1	59.401	0.004	25.116	0.303	0.053	0	7.093	6.916	0.732	99.618
AZU-003_L1_G1_C1	59.267	0.002	25.84	0.213	0.008	0.009	7.82	6.555	0.691	100.405
AZU-003_L1_G1_R1	57.562	0.078	26.368	0.258	0	0.036	8.589	6.268	0.671	99.83
AZU-003_L2_G2_C1	58.863	0.023	25.525	0.235	0	0.008	7.623	6.523	0.679	99.479
AZU-003_L2_G2_R1	52.58	0.027	29.421	0.633	0	0.077	12.696	3.978	0.256	99.668
AZU-003_L3_G3_C1	58.072	0	26.757	0.245	0	0.011	8.62	6.255	0.561	100.521
AZU-003_L3_G3_R1	58.399	0.006	26.471	0.287	0	0.006	8.323	6.185	0.576	100.253

Sample	SiO_2	TiO_2	Al_2O_3	FeO	MnO	MgO	CaO	Na_2O	K_2O	Total
AZU-003_L4_G4_C1	58.858	0.042	26.386	0.225	0	0	8.144	6.364	0.612	100.631
AZU-003_L4_G4_R1	56.282	0.013	27.219	0.386	0	0.02	9.563	5.701	0.493	99.677
AZU-003_L5_G5_C1	56.178	0.042	27.589	0.268	0	0.007	9.684	5.664	0.44	99.872
AZU-003_L5_G5_R1	58.336	0	25.69	0.259	0.043	0.026	8.071	6.483	0.701	99.609
AZU-004-PLG1-C1	58.298	0.036	25.756	0.222	0.009	0.014	7.966	6.58	0.779	99.66
AZU-004-PLG1-R2	58.6	0.038	25.831	0.394	0	0.039	7.786	6.315	0.917	99.92
AZU-004-PLG-C2	59.836	0.025	24.703	0.216	0.011	0.001	6.573	7.222	0.85	99.437
AZU-004-PLG2-R1	59.22	0.038	25.07	0.263	0	0.02	7.207	6.666	0.961	99.445
AZU-004-PLG3-C1	56.141	0	27.093	0.412	0	0.039	9.659	5.631	0.592	99.567
AZU-004-PLG3-R1	58.07	0.045	25.876	0.422	0.008	0.032	8.3	6.254	0.805	99.812
AZU-005-PLG1-C1	56.153	0.03	27.851	0.232	0	0.011	9.225	6.106	0.449	100.057
AZU-005-PLG1-R1	55.941	0	28.181	0.266	0	0.003	9.655	5.718	0.425	100.189
AZU-005-PLG1-R2	52.999	0.03	30.009	0.279	0.008	0	11.531	4.684	0.314	99.854
AZU-005-PLG2-C1	57.292	0.062	27.003	0.272	0.005	0.012	8.428	6.335	0.531	99.94
AZU-005-PLG2-C2	58.421	0.023	26.307	0.22	0.042	0.009	7.811	6.71	0.74	100.283
AZU-005-PLG4-C1	59.02	0	26.439	0.189	0.027	0.008	7.448	6.683	0.708	100.522
AZU-005-PLG4-R1	52.249	0.033	30.459	0.6	0	0.045	12.468	4.127	0.294	100.275
AZU-005-PLG5-C1	57.219	0.069	27.225	0.234	0	0.003	8.632	6.255	0.517	100.154
AZU-005-PLG5-R1	58.904	0.003	26.124	0.231	0	0	7.412	6.971	0.692	100.337
AZU-006-PLG1-C1	58.244	0	26.695	0.286	0.02	0	7.866	6.8	0.574	100.485
AZU-006-PLG1-R1	59.671	0.012	25.971	0.24	0.013	0.006	7.015	7.105	0.765	100.798
AZU-006-PLG2-C1	58.679	0	26.236	0.224	0	0.03	7.667	6.782	0.651	100.269
AZU-006-PLG2-R1	58.471	0.016	26.52	0.268	0.008	0.023	7.675	6.826	0.73	100.537
AZU-006-PLG3-C1	56.764	0.039	27.257	0.234	0.01	0	8.544	6.506	0.45	99.804
AZU-006-PLG3-R1	59.451	0.039	25.831	0.258	0.036	0.006	7.059	7.073	0.693	100.446
AZU-006-PLG4-C1	58.204	0	26.578	0.21	0.014	0	7.723	6.738	0.596	100.063
AZU-006-PLG4-R1	53.212	0.036	29.626	0.559	0.025	0.047	11.613	4.722	0.314	100.154
AZU-005-PLG2-R1	51.797	0.028	30.53	0.534	0.017	0.047	12.649	3.942	0.254	99.798

Sample	SiO_2	TiO_2	Al_2O_3	FeO	MnO	MgO	CaO	Na_2O	K_2O	Total
AZU-006-PLG2-R2	55.669	0.056	27.847	0.69	0	0.038	10.079	5.516	0.518	100.413
AZU-007-PLG1-C1	59.302	0.008	26.156	0.26	0	0.009	7.439	6.637	0.663	100.474
AZU-007-PLG1-R1	59.328	0	26.012	0.244	0	0.008	7.529	6.609	0.661	100.391
AZU-007-PLG2-C1	57.61	0.01	27.793	0.193	0.012	0	8.759	5.984	0.501	100.862
AZU-007-PLG2-R1	59.413	0	25.758	0.244	0.031	0.003	7.064	6.715	0.694	99.922
AZU-007-PLG3-C1	57.043	0	27.847	0.208	0	0.003	9.143	5.829	0.466	100.539
AZU-007-PLG3-C2	58.002	0.029	27.349	0.249	0.016	0.026	8.409	6.142	0.53	100.752
AZU-007-PLG3-R1	59.78	0.005	26.117	0.246	0.003	0.006	7.192	6.71	0.708	100.767
AZU-007-PLG4-C1	58.096	0.012	26.51	0.211	0	0.017	7.888	6.344	0.587	99.665
AZU-007-PLG4-R1	52.617	0.032	29.887	0.49	0.009	0.035	12.138	4.211	0.239	99.658
AZU-007-PLG5-C1	57.707	0.046	27.225	0.263	0	0.016	8.551	6.05	0.473	100.331
AZU-007-PLG5-R1	60.745	0.004	25.247	0.232	0	0.015	6.321	7.172	0.83	100.566
AZU-007-PLG5-R2	60.013	0	25.467	0.28	0	0	6.971	6.731	0.728	100.19
AZU-008-PLG1-C1	57.638	0	26.448	0.204	0.028	0.006	8.292	6.389	0.567	99.572
AZU-008-PLG1-R1	56.785	0.271	25.292	1.459	0.04	0.261	9.316	3.553	2.142	99.119
AZU-008-PLG2-c1	58.123	0	26.7	0.208	0.034	0.024	8.045	6.373	0.565	100.072
AZU-008-PLG2-R1	59.228	0	25.401	0.285	0	0.043	7.053	6.863	0.743	99.616
AZU-008-PLG3-C1	59.81	0	25.488	0.209	0	0	7.101	6.887	0.763	100.258
AZU-008-PLG3-R1	59.705	0.031	25.624	0.238	0.023	0.006	7.127	6.927	0.733	100.414
AZU-008-PLG4-C1	57.495	0.057	26.896	0.247	0	0.009	8.575	6.229	0.531	100.039
AZU-008-PLG4-R1	56.633	0.263	26.053	0.85	0.015	0.094	10.256	4.066	0.804	99.034
AZU-008-PLG5-C1	59.002	0.02	25.883	0.238	0.015	0.027	7.277	6.928	0.67	100.06
AZU-008-PLG5-R1	58.717	0.043	25.921	0.223	0	0.014	7.826	6.623	0.633	100
AZU-009-PLG1-C1	47.525	0.031	34.378	0.524	0.047	0.044	16.833	1.74	0.09	101.212
AZU-009-PLG2-C1	48.594	0.006	33.597	0.542	0	0.015	16.126	2.177	0.106	101.163
AZU-010-PLG1-C1	59.706	0	26.63	0.36	0.026	0	7.975	6.278	0.98	101.955
AZU-010-PLG2-C1	55.202	0.04	28.652	0.496	0	0.034	10.889	4.778	0.534	100.625
AZU-010-PLG2-R1	53.896	0.089	30.266	0.7	0.033	0.075	12.358	4.211	0.353	101.981

Sample	SiO_2	TiO_2	Al_2O_3	FeO	MnO	MgO	CaO	Na_2O	K_2O	Total
AZU-010-PLG2-R2	54.205	0.052	30.113	0.875	0	0.065	12.062	4.225	0.361	101.958
AZU-009-PLG1-C1	47.482	0.039	33.173	0.585	0.049	0.041	15.755	2.404	0.116	99.644
AZU-009-PLG1-R1	52.385	0.022	29.78	0.698	0	0.092	12.024	4.272	0.276	99.549
AZU-009-PLG2-C1	46.369	0.052	34.264	0.552	0.011	0.068	17.051	1.683	0.098	100.148
AZU-009-PLG2-R1	53.379	0.04	29.252	0.628	0	0.078	11.362	4.76	0.349	99.848
AZU-009-PLG3-C1	46.97	0.031	33.673	0.534	0.007	0.048	16.26	2.085	0.093	99.701
AZU-009-PLG3-R1	52.12	0.07	30.908	0.605	0	0.097	12.805	4.014	0.23	100.849
AZU-010-PLG3-R3	52.437	0.068	30.379	0.772	0	0.04	12.583	4.08	0.355	100.714
AZU-010-PLG1-C2	59.453	0.037	25.761	0.329	0.002	0.031	7.225	6.308	1.147	100.293
AZU-011-PLG1-C1	58.753	0.045	25.912	0.363	0	0.023	7.352	6.432	0.946	99.826
AZU-011-PLG1-R1	55.051	0	28.735	0.534	0.022	0.042	10.737	4.932	0.516	100.569
AZU-011-PLG2-C1	57.867	0.074	26.155	0.268	0	0.026	7.904	6.19	0.737	99.221
AZU-011-PLG2-R1	55.315	0.031	28.415	0.868	0.022	0.074	10.51	4.706	0.525	100.466
AZU-012-PLG1-C1	57.853	0.058	26.735	0.571	0	0.052	8.416	6.197	0.639	100.521
AZU-012-PLG2-C1	59.512	0.029	25.69	0.42	0.005	0.042	7.294	6.466	0.733	100.191
AZU-012-PLG2-R1	55.805	0	27.997	0.594	0	0.054	10.119	5.212	0.414	100.195

Table 11: Probe Data. Clinopyroxene

Sample	SiO_2	TiO_2	Al_2O_3	FeO	MnO	MgO	CaO	Na_2O	K_2O	Total
AZU-002-CPX-C1	50.455	0.68	3.293	7.816	0.406	15.476	19.985	0.675	0.01	98.81
AZU-002-CPX-C2	50.532	0.67	3.388	8.463	0.282	15.04	20.349	0.564	0.015	99.312
AZU-002-CPX-R1	50.869	0.581	3.542	6.947	0.168	15.923	20.24	0.362	0.019	98.733
AZU-002-CPX-R2	50.895	0.568	3.742	7.196	0.163	16.023	20.224	0.395	0.013	99.294
AZU-002-CPX2-C1	51.762	0.271	1.724	9.071	0.354	15.06	20.115	0.356	0.004	98.717
AZU-002-CPX2-C2	51.096	0.589	3.74	7.245	0.129	16.22	20.068	0.328	0.003	99.612
AZU-002-CPX2-R1	49.571	0.889	4.764	8.677	0.203	15.275	19.253	0.361	0.007	99.031
AZU-002-CPX3	50.236	0.833	3.41	10.394	0.344	14.349	19.304	0.454	0.01	99.372
AZU-002-CPX3-C2	52.98	0.186	1.908	9.145	0.508	14.487	19.891	0.429	0.114	99.649
AZU-003-CPX1-C1	58.088	0	26.97	0.238	0	0.01	8.559	5.394	0.532	99.791
AZU-003-CPX2-C1	51.881	0.464	3.049	9.036	0.235	16.583	18.908	0.394	0.008	100.588
AZU-003-CPX2-C2	50.547	0.687	4.777	7.555	0.139	15.367	20.128	0.44	0.02	99.925
AZU-003-CPX2-R1	51.459	0.582	3.949	7.82	0.154	15.623	20.096	0.369	0.019	100.071
AZU-003-CPX3-C1	49.982	0.834	5.291	8.153	0.175	15.462	19.44	0.434	0.015	99.908
AZU-003-CPX3-R1	51.364	0.47	3.514	7.402	0.153	16.228	20.174	0.45	0.007	99.802
AZU-004-CPX1-C1	52.44	0.269	1.222	8.781	0.421	15.111	20.528	0.416	0.015	99.203
AZU-004-CPX1-R1	52.553	0.269	1.281	8.613	0.34	15.186	20.51	0.433	0.012	99.197
AZU-004-CPX2-C1	50.614	0.661	3.491	8.156	0.205	15.001	20.195	0.434	0.021	99.008
AZU-004-CPX2-R1	52.55	0.344	1.685	8.678	0.376	15.069	20.14	0.465	0.154	99.461
AZU-004-CPX3-C1	51.578	0.595	2.718	8.866	0.21	15.88	19.426	0.397	0.014	99.869
AZU-004-CPX3-R1	52.619	0.285	1.313	8.372	0.331	15.412	20.753	0.418	0.018	99.524
AZU-004-CPX5-C1	52.645	0.309	1.623	8.734	0.451	15.091	20.417	0.428	0.022	99.762
AZU-004-CPX5-R1	52.72	0.278	1.224	8.41	0.405	15.218	20.877	0.375	0.016	99.523
AZU-005-CPX1-C1	52.12	0.405	2.121	7.844	0.185	16.612	19.733	0.284	0.009	99.355
AZU-005-CPX1-R1	51.863	0.462	2.8	6.824	0.144	16.655	19.991	0.31	0.009	99.317

Sample	SiO_2	TiO_2	Al_2O_3	FeO	MnO	MgO	CaO	Na_2O	K_2O	Total
AZU-005-CPX2-C1	51.714	0.54	3.033	7.119	0.195	16.619	20.124	0.302	0.008	99.757
AZU-005-CPX2-R1	52.133	0.451	2.288	6.983	0.201	16.931	20.044	0.262	0.019	99.448
AZU-006-CPX1-C1	53.699	0.112	0.267	6.737	0.119	16.897	21.053	0.286	0.006	99.176
AZU-006-CPX1-R1	50.151	0.751	4.161	7.947	0.202	17.082	17.931	0.342	0.038	99.053
AZU-006-CPX2-C1	57.158	0.449	4.642	5.625	0.144	12.076	14.121	0.263	0.561	95.099
AZU-006-CPX2-C2	50.902	0.534	3.399	6.671	0.16	17.056	19.788	0.349	0.025	99.283
AZU-007-CPX1-C1	47.539	1.589	7.643	12.22	0.396	15.644	11.038	1.316	0.528	97.94
AZU-007-CPX1-C2	47.545	1.313	7.69	14.615	0.33	13.984	11.429	1.401	0.781	99.088
AZU-008-CPX1-C1	45.783	1.471	8.993	14.351	0.35	12.597	11.086	1.939	1.145	97.715
AZU-008-CPX1-C3	42.604	3.147	12.435	12.749	0.139	14.189	10.97	2.264	0.621	99.149
AZU-008-CPX1-C4	45.519	1.834	8.856	14.282	0.546	13.896	10.911	1.698	0.567	98.133
AZU-007-C1	46.788	1.664	8.192	12.547	0.286	15.451	11.396	1.38	0.539	98.254
AZU-007-C2	46.536	1.635	8.028	12.375	0.337	15.556	11.542	1.45	0.574	98.033
JLAZU-007-CPX2-C1	53.744	0	29.923	0.595	0.046	0.085	11.237	4.904	0.289	100.823
JLAZU-007-CPX3-C1	52.046	0.035	30.817	0.603	0	0.084	12.841	4.017	0.218	100.661
JLAZU-007-CPX4-C1	50.643	0.006	32.446	0.584	0.016	0.01	14.395	3.306	0.185	101.591
JLAZU-007-CPX5-C1	51.3	0.043	31.454	0.599	0	0.085	13.481	3.706	0.182	100.867
JLAZU-009-CPX1-C1	49.343	0.816	5.545	7.537	0.116	15.357	21.171	0.31	0.009	100.317
JLAZU-008-CPX2-C1	49.091	1.408	8.858	13.41	0.379	12.076	12.578	1.709	1.07	100.579
JLAZU-008-CPX3-C1	46.108	1.43	7.894	14.618	0.393	13.966	11.603	1.405	0.864	98.281
JLAZU-010-CPX1-C1	52.781	0.184	1.115	9.108	0.408	15.151	21.102	0.384	0.013	100.25
JLAZU-010-CPX2-C1	52.866	0.117	0.957	8.652	0.718	15.13	21.732	0.365	0.016	100.553
JLAZU-011-CPX1-C1	52.499	0.197	1.081	8.753	0.533	15.091	22.082	0.385	0.005	100.626
JLAZU-011-CPX2-C1	52.854	0.156	0.925	8.554	0.69	15.213	21.856	0.4	0	100.648
JLAZU-007-CPX2-C1	49.652	0.84	5.084	7.315	0.196	15.467	20.353	0.398	0	99.622
JLAZU-007-CPX3-C1	54.504	0.175	1.386	13.326	0.22	29.759	1.678	0.038	0.002	101.123

Table 12: Probe Data, Orthopyroxene

Sample	SiO_2	TiO_2	Al_2O_3	FeO	MnO	MgO	CaO	Na_2O	K_2O	Total
AZU-001-OPX-C1	54.252	0.194	2.413	11.397	0.204	30.85	1.173	0.039	0.022	101.041
AZU-004-CPX4-C1	53.6	0.14	0.73	20.763	0.798	23.806	0.879	0.033	0.021	100.781
AZU-004-CPX4-R1	53.918	0.148	0.791	18.992	0.796	25.016	0.967	0.067	0.011	100.706
AZU-004-CPX4-R2	53.925	0.168	0.753	19.129	0.797	25.023	0.939	0.099	0.034	100.893
AZU-004-CPX4-C2	53.613	0.148	0.823	19.673	1.005	24.74	0.909	0.075	0.032	101.018
AZU-006-CPX3-C1	54.179	0.148	2.544	10.013	0.2	31.607	1.161	0.071	0.027	100.611
AZU-006-CPX3-R1	54.438	0.184	2.284	10.889	0.179	30.892	1.247	0.038	0.012	100.626
AZU-008-CPX1-C2	54.78	0.229	2.565	13.34	0.212	29.457	1.325	0.044	0.006	102.271
AZU-008-CPX1-C5	55.231	0.13	2.272	10.851	0.188	30.635	1.127	0.073	0.008	101.015
AZU-009-CPX1-C1	40.496	0	0.054	14.925	0.14	47.324	0.12	0.024	0.007	103.129
JLAZU-007-CPX1-C1	55.266	0.129	1.079	11.169	0.156	30.672	1.655	0.036	0.022	100.452
JLAZU-008-CPX1-C1	54.52	0.173	1.9	12.562	0.197	29.94	1.355	0.048	0.026	101.015
JLAZU-012-CPX1-C1	52.254	0.231	2.134	20.606	0.412	23.587	1.33	0.09	0.036	100.926
JLAZU-012-CPX2-C1	53.298	0.203	2.437	16.258	0.245	27.891	1.29	0.064	0.058	101.807
JLAZU-007-CPX1-C1	54.674	0.194	1.63	11.922	0.184	30.673	1.373	0.03	0.02	100.953
JLAZU-007-CPX4-C1	54.135	0.139	2.315	11.22	0.165	31.15	1.234	0.04	0	100.868

Sample	SiO_2	TiO_2	Al_2O_3	FeO	MnO	MgO	CaO	Na_2O	Total
AZU-001-OPX-C1	54.017	0.23	2.698	11.936	0.165	30.039	1.196	0.038	100.817
AZU-001-OPX-R1	53.868	0.226	2.001	14.998	0.269	27.96	1.223	0.041	100.637
AZU-001-OPX-C2	53.929	0.18	2.555	11.718	0.224	30.182	1.171	0.052	100.529
AZU-001-OPX-R2	55.051	0.214	1.841	11.536	0.211	30.679	1.26	0.058	101.201
AZU-001-OPX-C3	54.333	0.156	2.204	12.249	0.177	30.21	1.261	0.1	101.053
AZU-001-OPX-C4	54.686	0.156	1.893	11.685	0.26	30.365	1.222	0.055	100.684
AZU-001-OPX-R3	55.094	0.15	1.598	11.648	0.161	30.419	1.259	0.06	100.733
AZU-012-PX1-C1	53.373	0.266	2.569	17.378	0.32	26.973	1.211	0.069	102.16
AZU-012-PX1-C2	54.574	0.296	2.86	16.914	0.302	27.408	1.265	0.077	103.708

Table 13: Probe Data, Olivine

Sample	SiO_2	TiO_2	Al_2O_3	FeO	MnO	MgO	CaO	Cr_2O_3	NiO	Total
AZU-006-OL1-C1	39.555	0	0.004	14.576	0.183	44.88	0.116	0.05	0.169	99.533
AZU-006-OL1-R1	39.085	0	0.057	17.489	0.316	42.429	0.075	0.034	0.17	99.655
AZU-006-OL1-R2	52.185	0	28.928	0.807	0.016	0.073	12.374	0	0	94.383
AZU-009-OL1-C1	39.937	0.009	0.047	15.467	0.25	45.236	0.124	0.012	0.18	101.262
AZU-009-OL1-C2	40.25	0.015	0.037	15.801	0.237	44.803	0.108	0	0.124	101.375
AZU-009-OL1-C1	38.954	0	0.013	15.381	0.133	45.025	0.13	0.011	0.224	99.871
AZU-009-OL2-C1	39.452	0.001	0.028	14.629	0.238	45.588	0.123	0.002	0.179	100.24
AZU-010-OL1-C1	50.785	0.45	3.191	7.812	0.216	14.534	21.495	0.268	0.067	98.818
AZU-010-OL1-C2	52.445	0.176	1.017	8.482	0.632	14.483	21.852	0.013	0.05	99.15
AZU-010-OL1-C3	39.345	0.014	0.033	16.029	0.23	44.41	0.117	0.013	0.146	100.337
AZU-010-OL2-C1	51.993	0.171	1.21	9.2	0.687	14.277	21.373	0	0.006	98.917
AZU-011-OL1-C1	38.813	0.005	0.026	19.581	0.269	41.558	0.1	0.009	0.064	100.425
AZU-012-OL1-C1	51.74	0.197	2.051	20.178	0.347	23.348	1.301	0.226	0	99.388
AZU-009-OL3-C1	39.32	0	0.039	14.339	0.173	45.373	0.127	0.047	0.106	99.524
AZU-009-OL4-C1	53.362	0.186	0.945	18.04	0.429	25.339	1.039	0	0	99.34
AZU-008-OL1-C1	45.36	1.744	8.342	14.428	0.412	12.954	11.758	0	0.058	95.056
AZU-007-OL1-C1	43.447	2.648	9.708	14.121	0.278	12.387	10.934	0.005	0	93.528
JLAZU-008-OL1-C1	54.115	0.123	1.937	11.252	0.242	29.683	1.256	0.437	0.132	99.177
JLAZU-008-OL2-C1	53.163	0.234	2.559	11.554	0.188	28.549	1.669	0.429	0.034	98.379
JLAZU-008-OL3-C1	44.574	1.619	8.555	14.994	0.426	12.388	11.454	0	0.064	94.074

Table 14: Probe Data, Magnetite

Sample	TiO_2	Al_2O_3	FeO	MgO	Total
Comment	TiO2	Al2O3	FeO	MgO	Total
azu-010-MAG1	9.474	2.302	78.49	1.553	91.819
azu-010-MAG2	10.464	2.07	76.961	1.738	91.233
azu-010-MAG3	9.417	2.476	78.969	1.778	92.64
azu-011-MAG1	10.773	2.406	76.899	1.75	91.828
azu-011-MAG2	11.449	2.075	77.012	1.669	92.205
azu-011-MAG3	16.008	1.734	74.214	1.97	93.926
azu-012-MAG1	9.062	2.323	78.643	1.63	91.658
azu-012-MAG2	9.444	2.541	78.25	1.645	91.88
azu-012-MAG3	9.495	2.622	77.934	1.75	91.801
azu-001-MAG1	5.912	2.027	80.858	1.066	89.863
azu-001-MAG2	13.358	1.808	71.667	0.216	87.049
azu-001-MAG3	8.043	1.67	77.793	0.351	87.857
azu-002-MAG1	6.943	2.331	80.68	0.94	90.894
azu-002-MAG2	11.142	3.696	74.006	1.419	90.263
azu-002-MAG3	10.933	1.742	74.872	0.836	88.383
azu-003-MAG1	6.132	1.834	82.97	1.001	91.937
azu-003-MAG2	41.481	0.616	46.808	2.127	91.032
azu-003-MAG3	6.439	2.053	82.265	1.215	91.972
azu-004-MAG1	8.275	1.315	79.914	1.551	91.055
azu-004-MAG2	8.568	1.434	80.766	1.34	92.108
azu-004-MAG3	8.896	1.509	79.963	1.432	91.8
azu-005-MAG1	8.438	1.051	78.821	0.603	88.913
azu-005-MAG2	12.705	1.878	70.203	0.855	85.641
azu-005-MAG3	47.664	0.84	41.244	3.147	92.895

Sample	TiO_2	Al_2O_3	FeO	MgO	Total
azu-006-MAG1	8.275	2.194	79.675	1.151	91.295
azu-006-MAG2	7.601	2.262	80.419	1.102	91.384
azu-006-MAG3	9.658	2.032	79.034	1.163	91.887
azu-007-MAG1	7.324	2.693	78.954	1.407	90.378
azu-007-MAG2	7.318	2.816	70.498	1.066	81.698
azu-007-MAG3	5.191	1.893	81.463	1.414	89.961
azu-008-MAG1	4.03	2.563	63.034	0.68	70.307
azu-008-MAG2	6.462	2.273	80.874	0.871	90.48
azu-008-MAG3	6.824	2.15	80.914	1.109	90.997

Table 15: Partition Coefficients Used

JL-AZU-001

Element	Plagioclase	Clinopyroxene	Magnetite	Olivine	Orthopyroxene	Bulk D	D-1
U	0,34	0,04	0	0,002	0,023	0,220	-0,780
Ba	1	0,026	0	0,0099	0,013	0,625	-0,375
Nb	0,045	0,005	10	0,01	0,27	0,531	-0,469
Zr	0,048	1,11	0,71	0,14	0,18	0,244	-0,756
Y	0,2	1	0,2	0,01	0,54	0,371	-0,629
Sr	1,83	0,06	0	0,014	0,04	1,15	0,149
Rb	0,008	0,00175	0	0,001	0,01	0,007	-0,993
La	0,28	0,19	3	0,0067	0,26	0,384	-0,616
Ce	0,19	0,51	3	0,0083	0,47	0,412	-0,588
Eu	1,27	0,68	1,5	0,023	0,89	1,12	0,119
Yb	0,3	1,3	1,8	0,071	1,51	0,735	-0,265
V	0	1,35	26	0,06	0,6	1,46	0,464
Ni	0	5,9	29	36,4	5	3,34	2,34
Cr	0,016	9,7	153	0,7	0,95	8,35	7,35

JL-AZU-004

Element	Plagioclase	Clinopyroxene	Magnetite	Olivine	Orthopyroxene	Bulk D	D-1
U	0,01	0,04	0	0,002	0	0,012	-0,988
Ba	1,45	0,15	0,028	0,01	0,11	0,929	-0,071
Nb	0,045	0,005	0,7	0,01	0,27	0,101	-0,899
Zr	0,048	1,11	0,71	0,14	0,18	0,245	-0,755
Y	0,2	1	0,2	0,01	0,54	0,375	-0,625
Sr	2,41	0,12	0	0,014	0,21	1,53	0,530
Rb	0,008	0,00175	0	0,001	0,01	0,007	-0,993
La	0,28	0,19	3	0,0067	0,26	0,333	-0,667
Ce	0,19	0,51	3	0,012	0,47	0,365	-0,635
Eu	1,27	0,68	1,5	0,023	0,89	1,09	0,089
Yb	0,3	1,3	1,8	0,071	1,51	0,715	-0,285
V	0	1,35	26	0,06	0,6	1,04	0,043
Ni	0	4	29	2,2	5	2,42	1,42
Cr	0,016	10	153	0,7	0,95	5,94	4,94

JL-AZU-006

Element	Plagioclase	Clinopyroxene	Magnetite	Olivine	Orthopyroxene	Bulk D	D-1
U	0,01	0,04	0	0,002	0	0,016	-0,984
Ba	1,392	0,00162	0	0,0099	0,01	0,839	-0,161
Nb	0,045	0,005	0,7	0,01	0,27	0,061	-0,939
Zr	0,048	1,11	0,71	0,14	0,18	0,350	-0,650
Y	0,2	1	0,2	0,01	0,54	0,377	-0,623
Sr	1,943	0,06	0	0,014	0,04	1,18	0,185
Rb	0,008	0,00175	0	0,001	0,01	0,005	-0,995
La	0,28	0,19	3	0,0067	0,26	0,352	-0,648
Ce	0,19	0,51	3	0,0083	0,47	0,377	-0,623
Eu	1,27	0,68	1,5	0,023	0,89	1,00	0,002
Yb	0,3	1,3	1,8	0,071	1,51	0,590	-0,410
V	0	1,35	26	0,06	0,6	1,52	0,518
Ni	0	5,8	29	2,2	5	2,98	1,98
Cr	0	9,7	153	0,7	0,95	9,40	8,40

JL-AZU-008

Element	Plagioclase	Clinopyroxene	Magnetite	Olivine	Orthopyroxene	Bulk D	D-1
U	0,01	0,04	0	0,002	0	0,020	-0,980
Ba	1,42	0,026	0	0,0099	0,013	0,755	-0,245
Nb	0,045	0,005	10	0,01	0,27	0,063	-0,937
Zr	0,048	1,11	0,71	0,14	0,18	0,441	-0,559
Y	0,3	1	0,2	0,01	0,54	0,517	-0,483
Sr	2,16	0,06	0	0,014	0,04	1,16	0,155
Rb	0,008	0,00175	0	0,001	0,01	0,005	-0,995
La	0,28	0,19	3	0,0067	0,26	0,226	-0,774
Ce	0,3	0,51	3	0,012	0,47	0,352	-0,648
Eu	1,27	0,68	1,5	0,023	0,89	0,917	-0,083
Yb	0,3	1,3	1,8	0,071	1,51	0,637	-0,363
V	0	1,35	26	0,06	0,6	0,584	-0,416
Ni	0	7,69	29	36,4	5	7,03	6,03
Cr	0,016	10,3	153	0,7	0,95	4,32	3,32